



Intel® Model: 18265NGW

FCC ID: PD918265NG

Intel® Model 18265NGW Embedded Inside a notebook brand Dell Model P29S WiGig
Subsystem with RFEM 3

MPE Simulation Report

January 2018

Revision 1.0

Intel



Notice:

All information provided here is subject to change without notice. Contact your Intel representative to obtain the latest Intel product specifications and roadmaps.

Intel technologies' features and benefits depend on system configuration and may require enabled hardware, software or service activation. Performance varies depending on system configuration. No computer system can be absolutely secure. Check with your system manufacturer or retailer or learn more at [\[intel.com\]](http://intel.com).

Intel technologies may require enabled hardware, specific software, or services activation. Check with your system manufacturer or retailer.

You may not use or facilitate the use of this document in connection with any infringement or other legal analysis concerning Intel products described herein. You agree to grant Intel a non-exclusive, royalty-free license to any patent claim thereafter drafted which includes subject matter disclosed herein.

No license (express or implied, by estoppel or otherwise) to any intellectual property rights is granted by this document.

The products described may contain design defects or errors known as errata which may cause the product to deviate from published specifications. Current characterized errata are available on request.

Tests document performance of components on a particular test, in specific systems. Differences in hardware, software, or configuration will affect actual performance. Consult other sources of information to evaluate performance as you consider your purchase. For more complete information about performance and benchmark results, visit www.intel.com/benchmarks.

Copies of documents which have an order number and are referenced in this document may be obtained by calling 1-800-548-4725 or visit www.intel.com/design/literature.htm.

Intel, the Intel logo, {List of Intel trademarks} are trademarks of Intel Corporation or its subsidiaries in the U.S. and/or other countries.

*Other names and brands may be claimed as the property of others.

Copyright © 2018 Intel Corporation. All rights reserved.



Contents

| | |
|--|-----------|
| 1 Document Scope | 7 |
| 1.1 Introduction | 7 |
| 1.2 Associated Documents..... | 7 |
| 2 Background – WiGig System Operation | 8 |
| 2.1 System Block Diagram | 8 |
| 2.2 Beamforming | 9 |
| 2.3 TX Duty Cycle | 10 |
| 2.4 Intel 18265NGW module in Dell model P29S | 10 |
| 3 Beamforming Behavior in Operational Mode..... | 11 |
| 3.1 Introduction | 11 |
| 3.2 Environmental Conditions | 11 |
| 3.3 Test samples..... | 11 |
| 3.4 EUT Features | 11 |
| 3.5 Test System Description | 12 |
| 3.5.1 Antenna System and Measurement setup | 12 |
| 3.6 Test configuration | 14 |
| 3.7 Test results..... | 17 |
| 3.7.1 Case 1: EUT placed horizontally on lap | 17 |
| 3.7.2 Case 2: EUT placed horizontally with a lateral shifting to the side of the lap | 19 |
| 3.7.3 Case 3: EUT placed vertically on lap..... | 20 |
| 3.7.4 Case 4: EUT placed vertically with a lateral shifting to the side of the lap | 22 |
| 3.8 Conclusion | 24 |
| Appendix A: Supplemental Numerical Modeling for RF Exposure Power Density Evaluation..... | 25 |
| A.1 Platform Simulation Methodology..... | 25 |
| A.1.1 Assessment considerations | 25 |
| A.1.2 Near field results | 25 |
| A.1.3 Simulation tool | 26 |
| A.1.4 Finding the near-field, worst-case simulation configuration | 28 |
| A.1.5 3D models used in the simulation | 34 |
| A.1.6 Antenna feed | 38 |
| A.2 Power Density Simulation Results | 39 |
| A.2.1 Introduction | 39 |
| A.2.2 Simulation Results on the edge evaluation plane | 41 |
| A.2.3 Simulation Results on the base evaluation plane..... | 51 |
| A.2.4 Field and Power Density Distributions for the Six Highest Worst Cases | 61 |
| A.2.5 Conclusion | 68 |

List of Figures

| | |
|--|----|
| Figure 1 – Intel 18265NGW module system block diagram | 9 |
| Figure 2– RFEM 3 Subsets nominal beam directions (horizontal position) | 12 |
| Figure 3- RFEM 3 Subsets nominal beam directions (vertical position) | 13 |



| | |
|--|----|
| Figure 4– Qualitative measurement test setup | 14 |
| Figure 5– Qualitative measurement test configuration..... | 15 |
| Figure 6– Height variation for transition zone determination | 16 |
| Figure 7– Percentage of subset operation at d = 45 cm..... | 17 |
| Figure 8– Percentage of subset operation at d = 90 cm..... | 18 |
| Figure 9– Percentage of subset operation at d = 45 cm..... | 19 |
| Figure 10– Percentage of subset operation at d=90 cm | 20 |
| Figure 11– Percentage of subset operation at d = 45 cm | 21 |
| Figure 12– Percentage of subset operation at d = 90 cm..... | 22 |
| Figure 13– Percentage of subset operation at d=45 cm..... | 23 |
| Figure 14– Percentage of subset operation at d=90 cm | 23 |
| Figure 15 – Illustration of the adaptive mesh technique | 26 |
| Figure 16 – The x-y search on the edge and the base evaluation planes..... | 28 |
| Figure 17 – Near field worst-case terminology and orientation | 29 |
| Figure 18 – Worst-case evaluation plane for Dell model P29S platform | 34 |
| Figure 19 – Platform picture with RFEM 3 location | 35 |
| Figure 20 – Platform evaluation planes touching the body | 36 |
| Figure 21 – Channel 1 upper-bound, single-point power density- subset 1 | 47 |
| Figure 22 – Channel 1 single-point power density - subset 1..... | 48 |
| Figure 23 – Footprint of single-point power density plane representation..... | 48 |
| Figure 24 – 1-dimensional plots of the power density along x dimension | 49 |
| Figure 25 – 1-dimensional plots of the power density along y dimension | 49 |
| Figure 26 – Channel 1– spatially averaged power density over 1cm ² - subset 1 | 50 |
| Figure 27 – Channel 3 upper-bound, single-point power density- subset 3 | 57 |
| Figure 28 – Channel 3 single-point power density - subset 3..... | 58 |
| Figure 29 – Footprint of single-point power density plane representation..... | 58 |
| Figure 30 – 1-dimensional plots of the power density along x dimension | 59 |
| Figure 31 – 1-dimensional plots of the power density along y dimension | 59 |
| Figure 32 – Channel 1– spatially averaged power density over 1cm ² - subset 3 | 60 |

List of Tables

| | |
|---|----|
| Table 1 – Abbreviations..... | 5 |
| Table 2 – Subsets’ sectors | 13 |
| Table 3 – Test configuration summary – EUT placed horizontally on lap | 16 |
| Table 4 – WiGig channel frequencies..... | 39 |
| Table 5 – Power density simulation configuration and result details | 40 |
| Table 6 – Maximum upper bound single point power density [mW/cm ²] | 41 |
| Table 7 –Phases configurations for the first worst case for all antenna subsets..... | 43 |
| Table 8 –Phases configurations for the second worst case for all antenna subsets | 44 |
| Table 9 – Maximum single point power density [mW/cm ²] | 45 |
| Table 10 – Maximum spatially averaged power density over 1cm ² [mW/cm ²] | 46 |
| Table 11 – Worst-case power density – Subset 1..... | 50 |
| Table 12 – Maximum upper bound single point power density [mW/cm ²] | 51 |
| Table 13 –Phases configurations for the first worst case for all antenna subsets | 53 |
| Table 14 –Phases configurations for the second worst case for all antenna subsets..... | 54 |



| | |
|---|----|
| Table 15 – Maximum single point power density [mW/cm ²] | 55 |
| Table 16 – Maximum spatially averaged power density over 1cm ² [mW/cm ²] | 56 |
| Table 17 – Worst-case power density – Subset 3..... | 60 |
| Table 18 – Highest six worst-case spatially averaged power density | 61 |

List of Abbreviations

Table 1 – Abbreviations

| Abbreviation | Definition |
|---------------------|---|
| Ant | Antenna |
| Az | Azimuth |
| BB | Base Band |
| BF | Beam Forming |
| BT | Bluetooth |
| BW | Bandwidth |
| CPU | Central Processing Unit |
| EI | Elevation |
| EM | Electro-Magnetic |
| GHz | Gigahertz |
| IF | Intermediate Frequency |
| MAC | Media Access Control |
| M.2 | M2: Formerly known as Next Generation Form Factor (NGFF); used as specification for connectors of the expansion cards mounted on computer |
| mmWave | Millimeter Wave |
| PC | Personal Computer |
| PCIe | Peripheral Component Interconnect Express; a PCI Special Interest Group standard |
| R&D | Research and Development |
| RF | Radio Frequency |
| RFEM 3 | Third-generation Radio Front End Module |
| RFIC | Radio Frequency Integrated Circuit |
| RX | Receive |
| SKU | Stock Keeping Unit, specific product model version |
| SoC | System-on-Chip |



| Abbreviation | Definition |
|--------------|--|
| TDM | Time Division Multiplexing |
| TPC | Transmit Power Control |
| T/R SW | Transmit/Receive Switch |
| TX | Transmit |
| WiGig | Wireless Gigabit Alliance – the alliance that promoted the 60GHz into 802.11ad standard. |

Terms and Definitions

- **Subset:** A predefined group of radiating elements that are excited simultaneously with same amplitude and possibly different phases. There are three Subsets, and each one of them includes between 10 to 12 of the 24 elements of RFEM 3. The Subsets are also called Sub-Arrays.
- **Beamforming Code:** A configuration of phase-shifter values for all of the elements in a specific Subset. The Beamforming Code is used in order to direct the antenna to a desired spatial direction.
- **Sector:** A predefined set of Beamforming Codes, used for automatic selection of the Subset to be used.



1 Document Scope

1.1 Introduction

This report is submitted to support the compliance with the FCC rule located in Title 47 of the Code of Federal Regulations (CFR), parts §2.1093 and §15.255(f), of Intel 18265NGW WiGig module (FCC ID: PD918265NG), including an active antenna array, embedded inside the Dell model P29S.

Per the location of the active antenna array (a.k.a. RFEM 3) in the Dell model P29S platform, the distance between the antenna arrays to the body of an end user, at the closest contact point, will be in the near field.

In order to prove that during typical use the energy goes in most cases away from the human body, several tests of beamforming behavior were performed under different use cases conditions. The results are presented in this document.

These tests are supported by a determination of the near-field power average density performed using an EM simulation supported by a near field measurement. An EM simulation that includes the RFEM 3 transmitter model embedded inside the Dell model P29S is used to determine the worst case configuration and the correspondent near field power density. This worst case power density is considered as a conservative case because the energy is always oriented toward the human body, this latter is also supported by near field measurements. Due to the range of variations and uncertainty introduced by measurement and simulation, the results can only be applied to supplement each other, in conjunction with the beamforming mitigation results, through qualitative comparison and extrapolation to establish compliance at the device surface.

The simulation method and simulation results are described in this document. The near field measurement system details are described in document [2] and the comparison between simulation and measurement is shown in [3].

Chapter 2 provides relevant background on Intel 18265NGW module. Chapter 3 shows the results of the beamforming behavior in operational mode directing the energy away from body. Appendix A describes the simulation methodology to determine the worst case configuration and the power density simulation results.

1.2 Associated Documents

This 'MPE Simulation Report' and the called references [2] and [3] are not confidential; relevant details and explanations that qualify for confidentiality are included separately in the operational description document called reference [1]

[1] "170512-Dell P29S - Theory of Operation Report"

[2] "170512-Dell P29S - Near Field Measurement Report "

[3] "170512-Dell P29S - Simulations and Measurements Comparisons and Compliance Descriptions Report"



2 Background – WiGig System Operation

2.1 System Block Diagram

The Intel 18265NGW module is a solution for WiGig connectivity for various platforms. The Intel 18265NGW module can be embedded in a conventional clamshell PC (such as the Dell model P29S) as well as in modern 2-in-1 (detachable) platforms and tablet-like platforms.

The client solution for Dell P29S includes the 18265NGW WiGig module (FCC ID: PD918265NG) connected to a beam forming antenna array RFEM 3 using one IF coaxial cable.

The WiGig module (FCC ID: PD918265NG) is a PCIe M.2 module consisting of a WiGig BB chip, which implements the WiGig MAC, Modem, BF algorithm, and active antenna array module control, as well as the BB + IF stage circuitry. Intel calls this module Oak Peak. (Note that Oak Peak uses the same WiGig base band silicon as Maple Peak.)

RFEM 3 (10101RRFW) is an active antenna array module, which converts the IF signal to a 60 GHz signal. It also performs the beam forming functionality by phase¹ shifting the RF signal that goes to each antenna. The RFEM 3 is slave to the WiGig BB chip, since all module control and algorithms run on the BB chip.

Intel System-on-Chip (SoC) houses the central processing unit (CPU), which executes applications and provides command and control of the client solution, including all I/O data and addressing.

¹ Each antenna is excited by an amplitude at a defined phase angle. RFEM 3 feeding circuit has 2 bit phase shifter. Therefore, the phase's values can be 0, 90, 180, or 270 degrees.

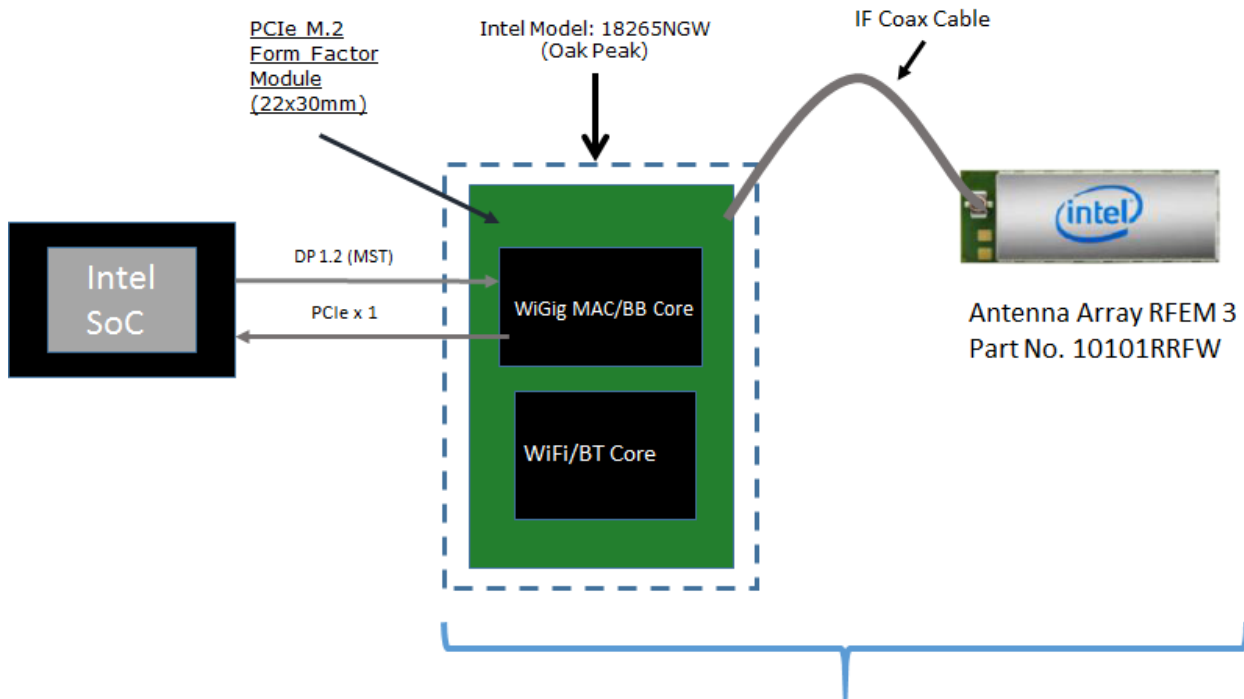


Figure 1 – Intel 18265NGW module system block diagram

Note: Also known by Intel internal project code name “Oak Peak,” the above-described WiGig module solution still uses the “Maple Peak” Intel chipset (both MAC/BB chip and radio chip).

2.2 Beamforming

Achieving high-bandwidth communication over 60 GHz channels usually requires directional antennas at the transmitter and receiver sides. In consumer electronics, fixed directional or mechanically-rotated antennas are not practical, and electronically steerable antennas are usually used.

In the Intel 18265NGW module, an electronically-steerable antenna array is used. Beam forming protocol (defined in the IEEE 802.11ad standard) is used to find the right direction for setting both the RX and TX antenna directions.

Due to the RFEM structure, it is not easy to predict the direction and beam forming combination that yields the maximum energy in near field. To find this value, a search over the possible beam forming combination was made and the worst case value was taken. A detailed explanation of this process can be found in Section A.1.4.



2.3 TX Duty Cycle

The WiGig protocol, as defined in ISO/IEC/IEEE 8802-11:2012/Amd.3:2014(E), Clause 21, is packet-based, with time division multiplexing (TDM). The Intel 18265NGW module is configured to guarantee that the TX-Duty-Cycle, defined as the ratio of the duration of all transmissions to the total time, is at most 70% over any 10-second period. This was established by worst-case analysis, as derived from full-system simulation, and verified by measurements.

The limited TX-Duty-Cycle is established based on HW and FW implementation with a measurement interval of ~100 ms (102.4 ms) and 10-second averaging; other details are provided in reference [1]. The 70% duty cycle limitation is guaranteed, independent of user activity, and therefore adheres to the source-based time-averaging definition in Title 47 of the Code of Federal Regulations (CFR) 2.1093(d)(5).

In addition, measurements of the Intel 18265NGW module, configured to obtain maximal TX-Duty-Cycle in a fully loaded system, resulted in an actual maximum TX-Duty-Cycle of 58% over any 10-second period, lower than the upper bound derived from the analysis in this section.

2.4 Intel 18265NGW module in Dell model P29S

Intel produces several HW SKUs (variations) of the Intel 18265NGW module, which target different types of customer platform products.

Dell uses the Intel 18265NGW module inside the Dell model P29S platform. This SKU is characterized by

1. Supporting channels **1+2+3**
2. Reduced power emission, which translates to
 - a. Maximum transmit conducted power of **6.5 dBm** aggregated conducted power at the antenna ports.
 - b. Maximum TX duty-cycle of **70%**.



3 Beamforming Behavior in Operational Mode

3.1 Introduction

The goal of this section is to show that during typical use of RFEM 3 inside Dell Model P29S, the energy would go away from the human body. This will be showed by performing several beamforming behaviour tests taking into account different typical heights, distances and EUT orientation.

3.2 Environmental Conditions

At the site where the measurements were performed the following limits were not exceeded during the tests:

| | |
|-------------|------------|
| Temperature | 21°C ± 1°C |
| Humidity | 30% ± 10% |

3.3 Test samples

| Sample | Control # | Description | Model | Serial Number | Date of receipt |
|--------|---------------|--|----------------------|------------------------------|-----------------|
| #01 | 170512-01.S01 | Wireless Module installed in conventional laptop | 18265NGW inside P29S | N/A | 2017-05-11 |
| | 170512-01.S01 | AC Adapter | NA | CN-02YK0F-LOC00-6BS-0192-A00 | 2017-05-11 |
| #02 | 170228-01.S14 | Dock Station | WIDOCK-SDS | EZWI511001 84 | 2017-05-11 |
| | 170228-01.S14 | AC Adapter | NA | NA | 2017-05-11 |

3.4 EUT Features

| | | |
|-------------------------------|--|--|
| Brand Name | Intel Model 18265 inside Dell Model P29S | |
| Model Name | Client Platform Design Guidelines | |
| FCC/IC ID | PD918265NG/IC ID: 1000M-18265NG | |
| Software Version | 3.0.41131.1 | |
| Prototype / Production | Production | |
| Host Identification | P29S series | |
| Exposure Conditions | Localized free space power density | |
| Supported Radios | WiGig | 60GHz (57.24 – 63.72 GHz) |
| | 802.11b/g/n | 2.4GHz (2400.0 – 2483.5 MHz) |
| | 802.11a/n/ac | 5.2GHz (5150.0 – 5250.0 MHz) 5.3GHz (5250.0 – 5350.0 MHz) 5.6GHz (5470.0 – 5725.0 MHz) 5.8GHz (5725.0 – 5825.0 MHz) |
| | Bluetooth | 2.4GHz (2400.0 – 2483.5 MHz) |
| | Antenna Information | RFEM3 (10101RRFW) |

Note: RF exposure compliance for 802.11 and Bluetooth capabilities are not addressed in this document neither the associated documents mentioned in section 1.2.

3.5 Test System Description

As mentioned in the introduction, the goal of this measurement is to prove that energy goes away from the body when the EUT is at its proximity. The metric that can show this behaviour is the percentage of operation of each subset.

The Dell Model P29S is a convertible PC, the tests are performed, in tablet mode (Lid open at 360° as shown in Figure 18), with four EUT orientations:

- Case 1: EUT placed horizontally over lap.
- Case 2: EUT placed horizontally with a lateral shifting to the side of the lap.
- Case 3: EUT placed vertically over lap..

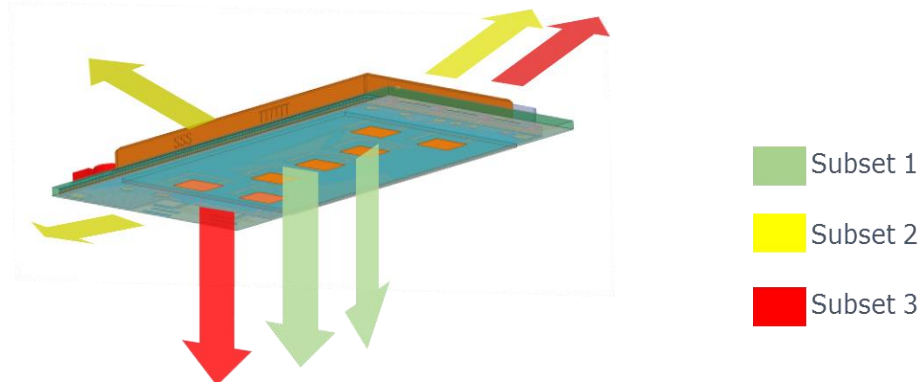
Case 4: EUT placed vertically with a lateral shifting to the side of the lap.

The next sections, present the test setup, test configuration and measurement results for the four cases listed above.

3.5.1 Antenna System and Measurement setup

3.5.1.1 Antenna System

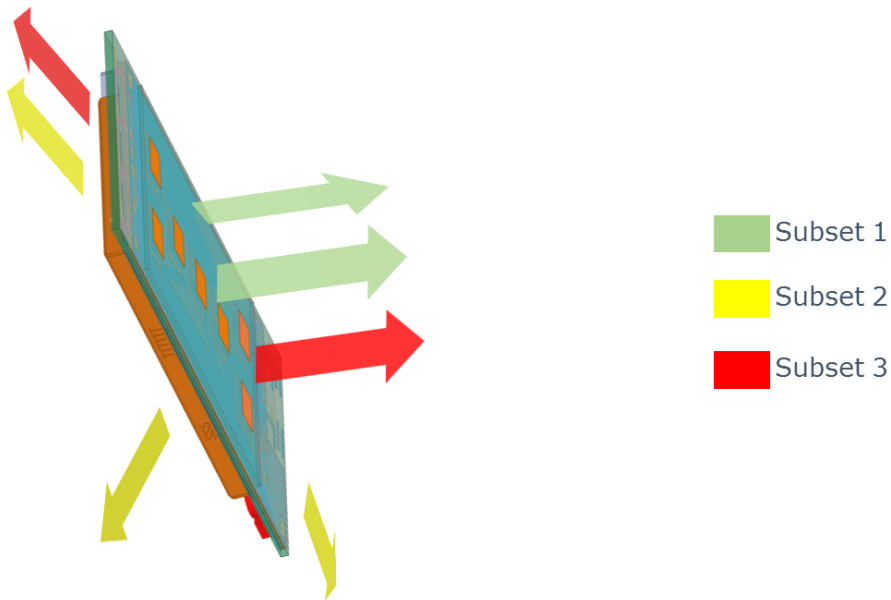
Figure 2 illustrates the position of the RFEM 3 antenna when the EUT is placed horizontally over lap (Case 1 and Case 2). The same figure shows the nominal beam direction of each subset. In this case, the tests should prove that subset 2 is operational in the majority of time when the DUT is close to the body in order to direct the beam away. The test configurations of this case are mentioned in Table 3.



- Subset 2 directed away from the body
- Subset 1 and Subset 3 directed toward the body

Figure 2– RFEM 3 Subsets nominal beam directions (horizontal position)

In the cases when the EUT is vertically placed over laps (Case 3 and Case 4), the PC edge is touching the body and the tests should prove that subset 1 or subset 3 is operational in the majority of time when the DUT is close to the body in order to direct the beam away. Figure 3 shows the position of the RFEM 3 antenna when the EUT is vertically placed over laps. The test configurations of this case are mentioned in Table 3.



- Subset 2 directed toward the body
- Subset 1 and Subset 3 directed away from the body

Figure 3– RFEM 3 Subsets nominal beam directions (vertical position)

Note that when a subset is operational, a beamforming code (phases' combination of the subset's elements) among a set of codes (instances) for each subset is realized.

Table 2 illustrates the sectors numbers associated to each subset. The 62 sectors were designed to achieve sufficient coverage in all spatial directions.

Table 2 – Subsets' sectors

| Number of Sector | | | | | | | | | | | | | | | |
|------------------|----|----|----|----------|----|----|----|----------|----|----|----|----|----|----|----|
| 1 | 2 | 3 | 4 | 5 | 6 | 7 | 8 | 9 | 10 | 11 | 12 | 13 | 14 | 15 | 16 |
| 17 | 18 | 19 | 20 | 21 | 22 | 23 | 24 | 25 | 26 | 27 | 28 | 29 | 30 | 31 | 32 |
| 33 | 34 | 35 | 36 | 37 | 38 | 39 | 40 | 41 | 42 | 43 | 44 | 45 | 46 | 47 | 48 |
| 49 | 50 | 51 | 52 | 53 | 54 | 55 | 56 | 57 | 58 | 59 | 60 | 61 | 62 | | |
| Subset 1 | | | | Subset 2 | | | | Subset 3 | | | | | | | |

The second parameter to be studied in these tests is the existence of a transition zone in which a handover from subset to another is observed. This is essential to prove the efficiency of the beamforming algorithm.

3.5.1.2 Measurement Setup

- The dock station is placed on the table with a height of 80 cm above the horizontal office floor.
- The person is holding the EUT horizontally on his lap.
- Initially, the EUT is touching the person's lap at the evaluation plane as shown in Figure 4. In this case, the dock station and the EUT are at the same height i.e. 80 cm above the horizontal office floor.

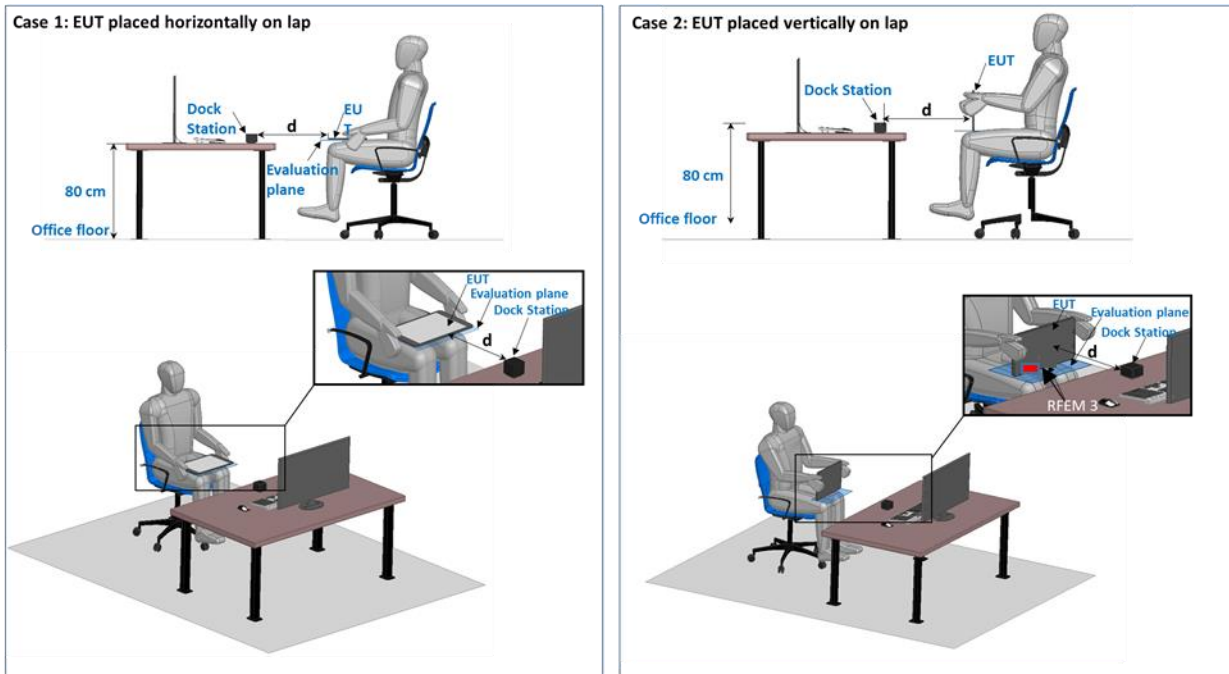


Figure 4– Qualitative measurement test setup

3.6 Test configuration

For each test case, the test configuration is described as follow:

- The EUT and the dock station are set in operational mode and a link condition between the two devices is made using a link software used with Dock and host model P29S in normal operational mode (Wireless Dock Manager, Version 3.0.41131.1).
- The measurement is performed at two distances (d) between the dock station and the EUT i.e. 45 cm and 90 cm. These distances represent two typical use cases of the Laptop.
- For each distance (d) the test is performed for several heights (h) between the EUT exposure's plane with and without a horizontal offset (lateral shifting) of the platform to the side of the user's lap. The height is modified (Figure 6) as described below
 - (1) The EUT is raised from the lap position ($h=0$) until a transition height ($h=h_t$) where a handover between subsets is observed, if applicable. The handover is a drop of % below 80% for the given subset.

- (2) The EUT height is increased until it has passed the transition region in which a handover from a subset to another is observed
- (3) The EUT is moved back toward the lap in reverse order until it has passed the lower boundary of the transition region.
- Styrofoam spacers with specific heights are used between the EUT and the person lap's (Figure 5)
- Beam forming triggering in operational mode: when the link is not in maximum MCS¹ (MCS 12) the SW triggers beam forming each 4 seconds.
- In case of abrupt MCS degradation (3 MCS steps) compared to the chosen MCS, or no response from the other side, then there is immediate beam forming triggering. For each EUT position, the measurement time is selected to be sufficient for conditions to stabilize and to record the beamforming code instances. When connection is dropped, the device starts a search phase in which it normally transmits for less than 1ms once per 1 second (<0.1%). Additional transmissions happen only if it finds another device and they start to connect to each other.

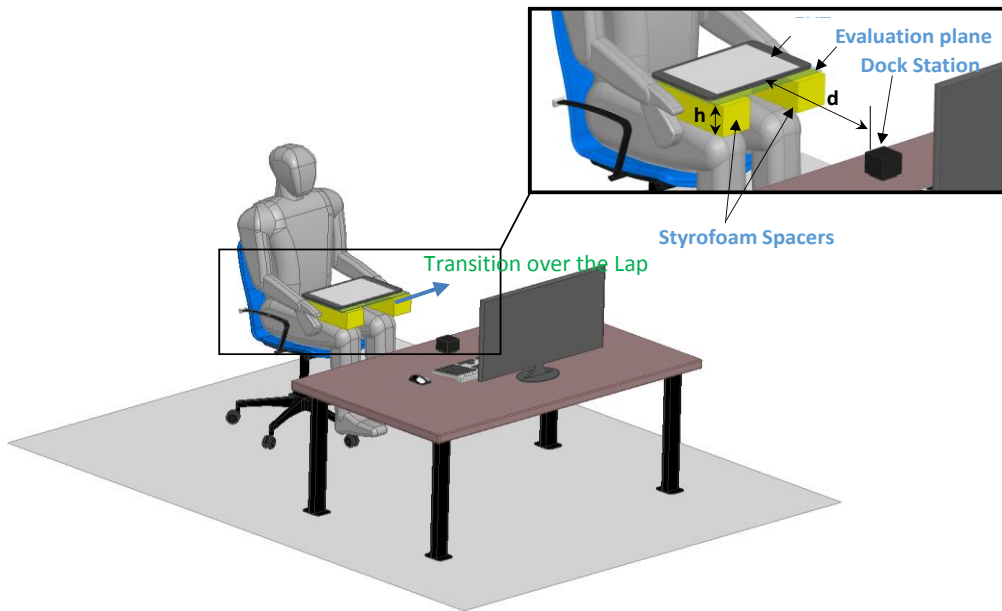


Figure 5– Qualitative measurement test configuration

1: MCS stands for Modulation and Coding Scheme, and it controls the PHY data rate being used per packet. Data MCS ranges between 1 and 12, and the higher the MCS is the higher data rate. The beamforming aims to improve the link conditions. If the MCS is MCS-12, then data-rate is maximal, there's no option to further improve the link, and therefore beamforming is not triggered.

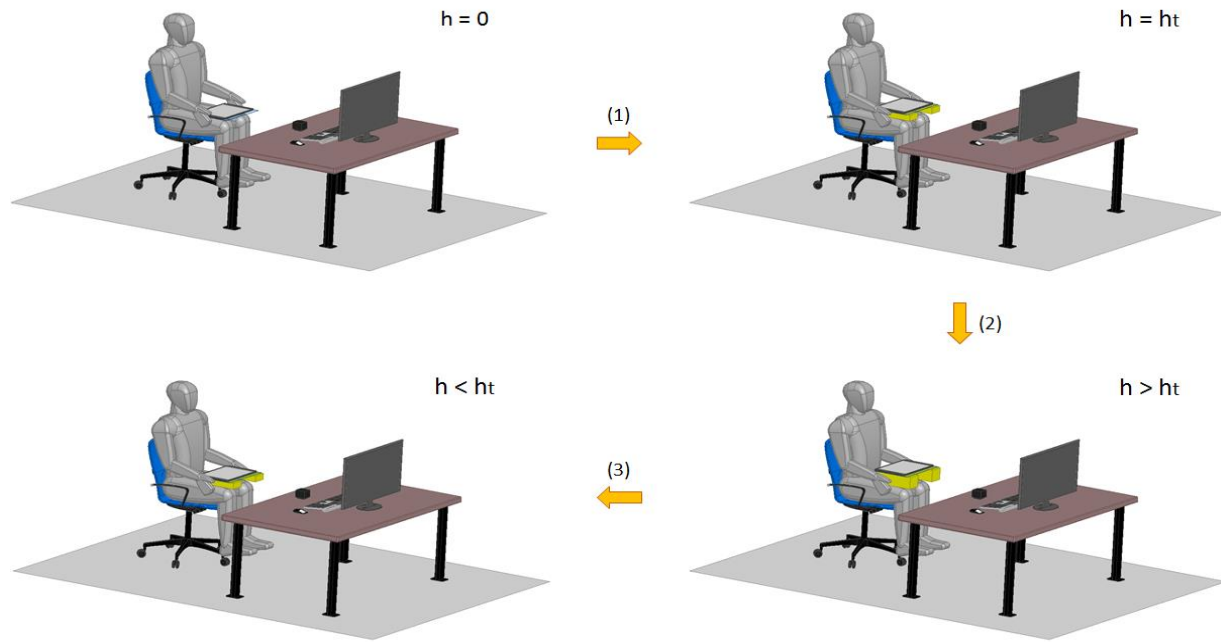


Figure 6– Height variation for transition zone determination

Table 3 summarizes the realized test configurations:

Table 3 – Test configuration summary – EUT placed horizontally on lap

| Test number | EUT to dock station distance (d) | Transverse transition | Position | EUT to person laps distance (h) |
|-------------|----------------------------------|-----------------------|------------|--|
| 1 | 45 cm | No | Horizontal | 0, 1, 2, 4, 6, 8, 10, 12, 14, 16 and 20 cm |
| 2 | 90 cm | No | Horizontal | 0, 1, 2, 4, 6, 8, 10, 12, 14, 16 and 20 cm |
| 3 | 45 cm | Yes | Horizontal | 0, 1, 2, 4, 6, 8, 10, 12, 14, 16 and 20 cm |
| 4 | 90 cm | Yes | Horizontal | 0, 1, 2, 4, 6, 8, 10, 12, 14, 16 and 20 cm |
| 5 | 45 cm | No | Vertical | 0, 2, 4, 6, 8, 10, 12, 14, 16 and 20 cm |
| 6 | 90 cm | No | Vertical | 0, 2, 4, 6, 8, 10, 12, 14, 16 and 20 cm |
| 7 | 45 cm | Yes | Vertical | 0, 2, 4, 6, 8, 10, 12, 14, 16 and 20 cm |
| 8 | 90 cm | Yes | Vertical | 0, 2, 4, 6, 8, 10, 12, 14, 16 and 20 cm |

3.7 Test results

3.7.1 Case 1: EUT placed horizontally on lap

Figure 7 and Figure 8 show the test results of the subset operation according to the EUT to lap distance (h), for the two horizontal distances: 45 and 90 cm respectively, when the EUT is placed horizontally on the lap. The x-axis represents the height above lap while the y-axis represents, for each subset, the percentage of subset operation.

For every measurement point i.e. every h, the total percentage of instances for three subsets is 100%. The 100% of y-axis applies separately for each translation direction. For example, for a given h, if we have 100 beamforming instances, and among these instances we have 90 instances where sub-array 2 is operational , 8 instances where sub-array 3 is operational, 2 instances for sub-array 1, then the percentage of sub-arrays 1, 2 and 3 are 2%, 90% and 8% respectively.

Test 1 results at 45 cm distance

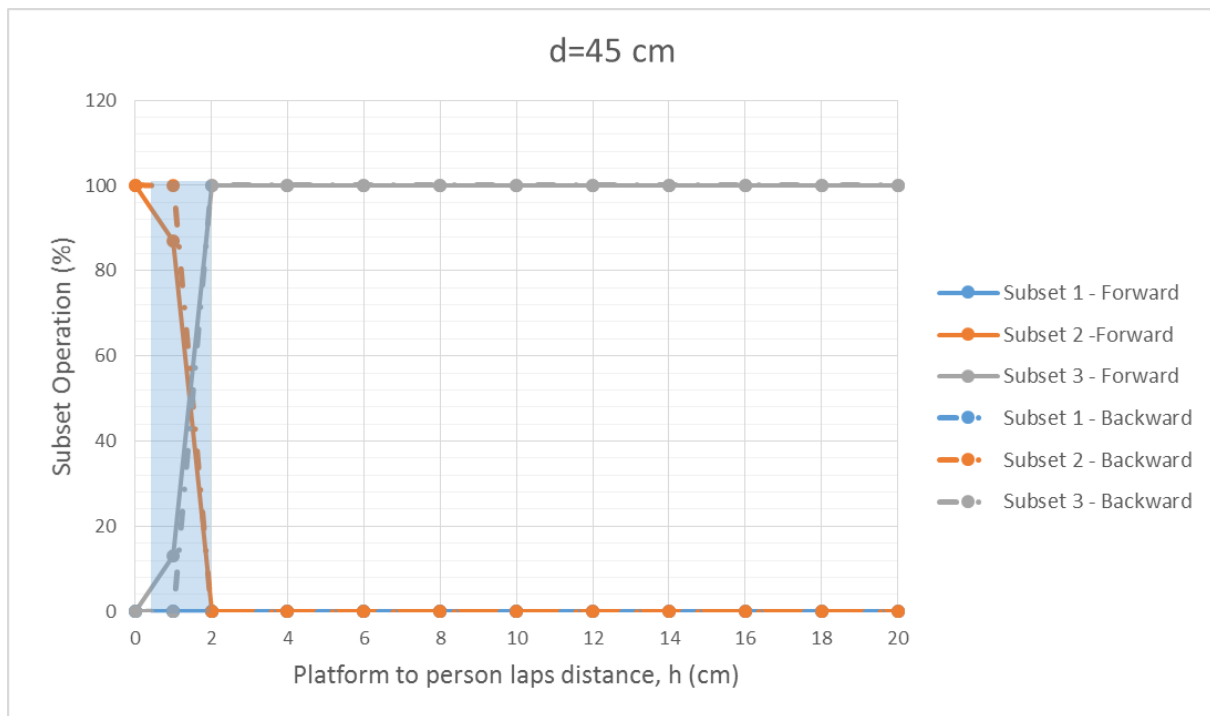


Figure 7– Percentage of subset operation at d = 45 cm

Test 2 results at 90 cm distance

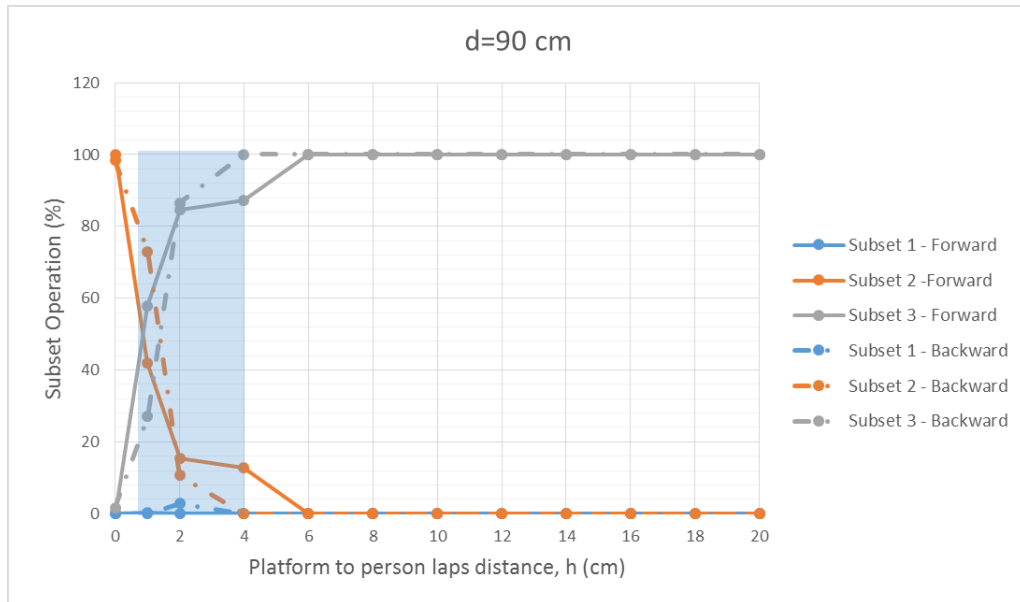


Figure 8– Percentage of subset operation at $d = 90$ cm

Figure 7 and Figure 8 presents the results of the mitigation test when the user is holding the EUT horizontally on his lap and is placed at a distance of 45 cm and 90 cm from the Docking Station. When the platform touch the body (at $h=0$ cm), subset 2 is 100% operational among the three subsets. A transition zone is observed when h is vary between 1-2cm and 1-4cm at 45 and 90 cm horizontal distance respectively. This transition zone is a drop of % below 80% for subset 2. Subset 3 is always selected for h greater than 2 cm and 4 cm at 45 and 90 cm horizontal distance respectively.

This shows that that the beam steering algorithm behaves in such a manner as to direct the energy away from the body.

Note that in this horizontal position, when the platform touches the person laps ($h=0$), the distance between the RFEM 3 and the lap is 16 mm (Figure 20). Therefore, the transition zone is observed when the RFEM 3 antenna is between 26-36 mm and 26-56 mm from the body at 45 cm and 90 cm horizontal distance respectively.

Note: In this EUT position and when the transition region is passed, subset 3 is operational almost all the time rather than subset 1. This is related to a better link budget between the RFEM 3 and the dock station established by subset 3 in this EUT position. Indeed, from a side the dock station antennas are vertically polarized, and from the other side subset 3 is composed by eleven vertically polarized elements while subset 1 contain only four vertically polarized elements. That's why subset 3 is active not subset 1. Therefore a scenario where subset 1 could be active is when the EUT is rotated of 90 degrees (the EUT screen become in portrait mode). In this case, the subset 1 polarization ensure better link budget than subset 3. In all cases the energy will be directed away from body.

3.7.2 Case 2: EUT placed horizontally with a lateral shifting to the side of the lap

Figure 9 and Figure 10 show the test results of the subset operation according to the EUT to lap distance (h), for the two horizontal distances: 45 and 90 cm respectively. The EUT is placed horizontally with a lateral shifting to the side of the Lap.

The x-axis represents the height above lap while the y-axis represents, for each subset, the percentage of subset operation.

Test 1 results at 45 cm distance

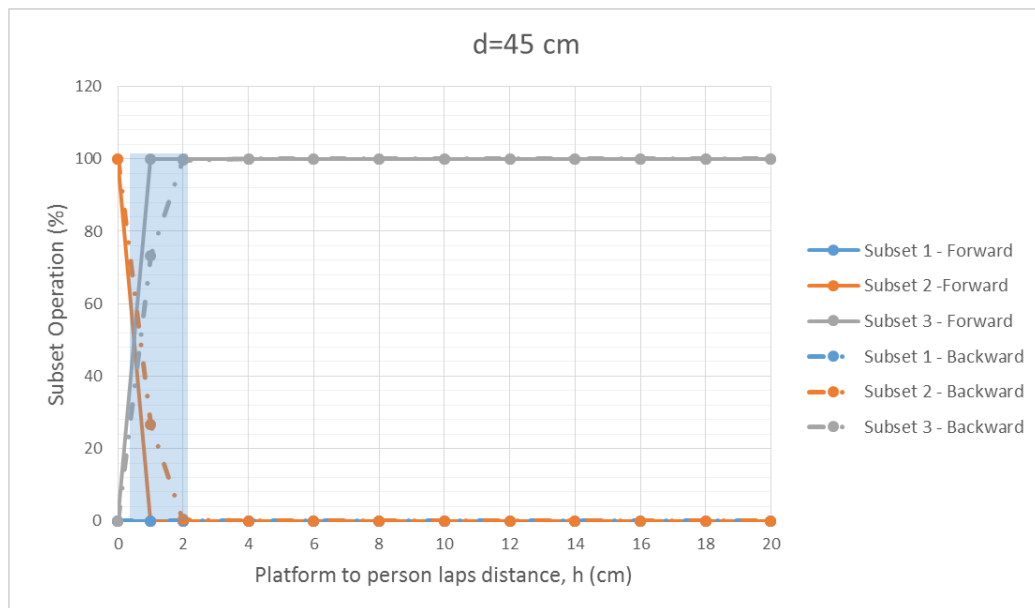


Figure 9– Percentage of subset operation at $d = 45$ cm

Test 2 results at 90 cm distance

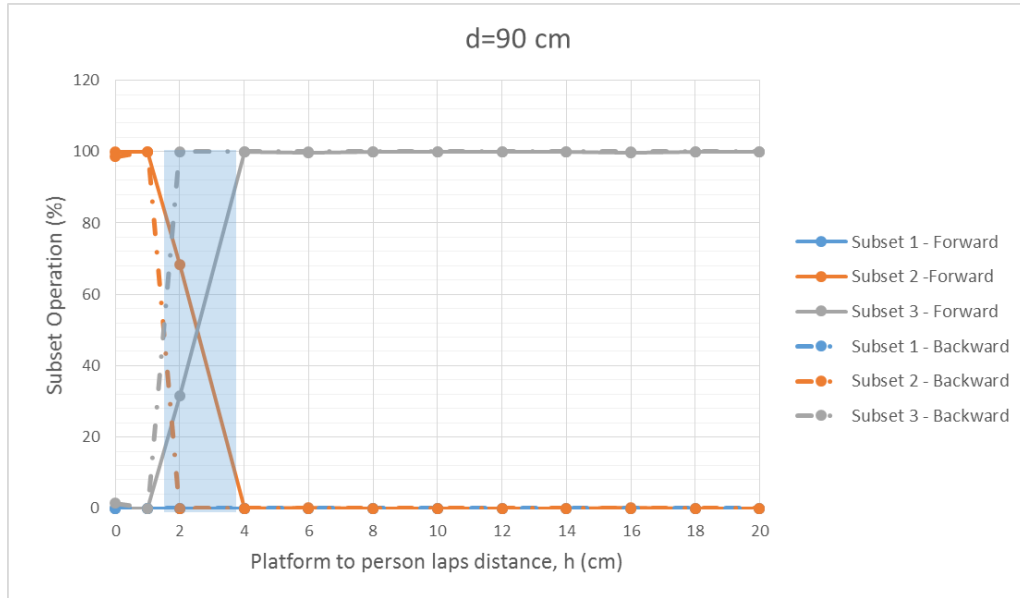


Figure 10– Percentage of subset operation at d=90 cm

Figure 9 and Figure 10 presents the results of the mitigation test when the user is holding the EUT horizontally on his lap and is placed at a distance of 45 cm and 90 cm from the Docking Station. When the platform touch the body (at h=0cm), subset 2 is 100% operational among the three subsets. A transition zone is observed when h is vary between 1-2cm and 2-4cm at 45 and 90 cm horizontal distance respectively. This transition zone is a drop of % below 80% for subset 2. Subset 3 is always selected for h greater than 2 cm and 4 cm at 45 and 90 cm horizontal distance respectively.

This shows that that the beam steering algorithm behaves in such a manner as to direct the energy away from the body.

Note that in this horizontal position, when the platform touches the person laps (h=0), the distance between the RFEM 3 and the lap is 16 mm (Figure 20). Therefore, the transition zone is observed when the RFEM 3 antenna is between 26-36 mm and 36-56 mm from the body at 45 cm and 90 cm horizontal distance respectively.

Note: In this EUT position and when the transition region is passed, subset 3 is operational almost all the time rather than subset 1. This is related to a better link budget between the RFEM 3 and the dock station established by subset 3 in this EUT position. Indeed, from a side the dock station antennas are vertically polarized, and from the other side subset 3 is composed by eleven vertically polarized elements while subset 1 contain only four vertically polarized elements. That's why subset 3 is active not subset 1. Therefore a scenario where subset 1 could be active is when the EUT is rotated of 90 degrees (the EUT screen become in portrait mode). In this case, the subset 1 polarization ensure better link budget than subset 3. In all cases the energy will be directed away from body.

3.7.3 Case 3: EUT placed vertically on lap

Figure 11 and Figure 12 show the test results of the subset operation according to the EUT to lap distance (h), for the two horizontal distances: 45 and 90 cm respectively when the

EUT is placed vertically over the lap. The x-axis represents the height above lap while the y-axis represents, for each subset, the percentage of subset operation.

Test 1 results at 45 cm distance

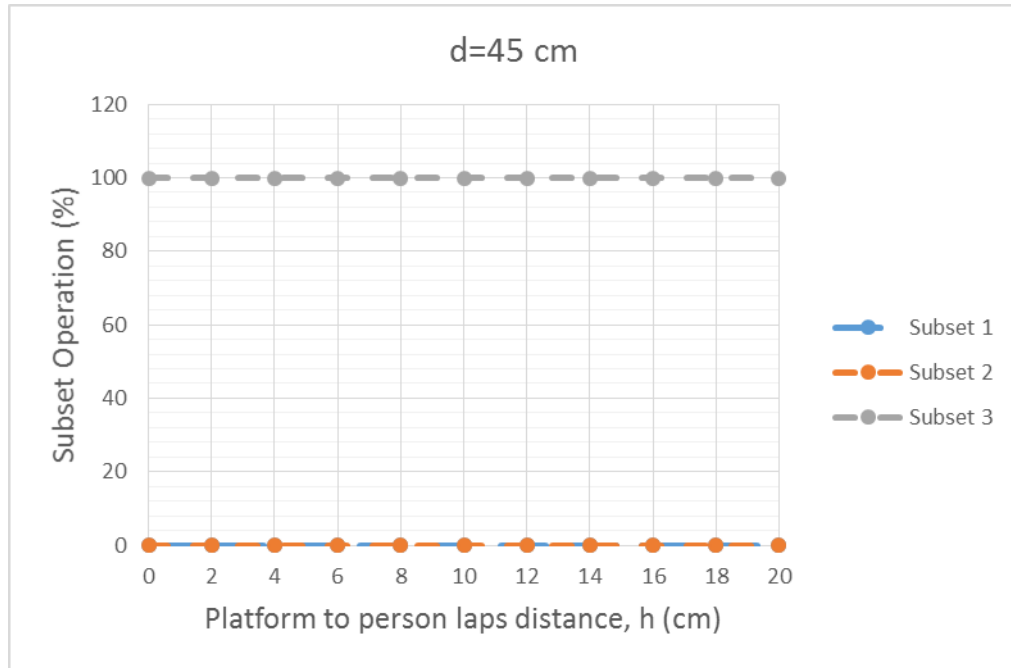


Figure 11– Percentage of subset operation at $d = 45$ cm

Test 2 results at 90 cm distance

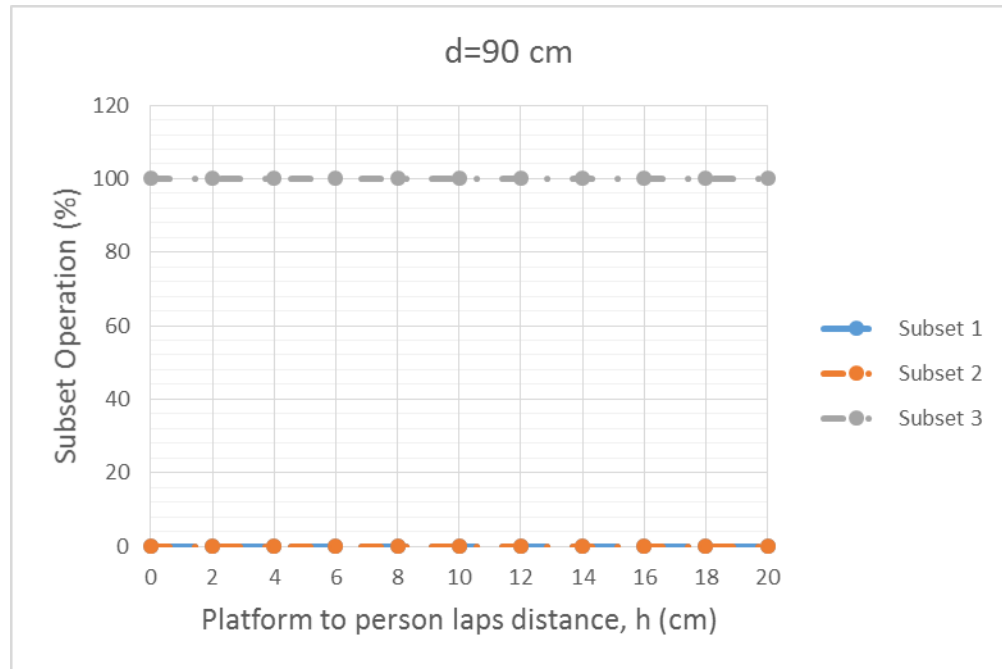


Figure 12– Percentage of subset operation at $d = 90$ cm

Figure 11 and Figure 12 present the results of the mitigation test when the user is holding the EUT vertically on his lap and is placed at a distance of 45 cm and 90 cm from the Docking Station. For h going from 0 cm to 20 cm subset 3 is 100% operational among the three subsets. The transition region is not observed in this test case since the subset 3 is 100% operational for all heights.

This shows that the beam steering algorithm behaves in such a manner as to direct the energy away from the body by selecting only subset 3.

Note: In this EUT position, subset 3 is operational almost all the time rather than subset 1. This is related to a better link budget between the RFEM 3 and the dock station established by subset 3 in this EUT position. Indeed, from a side the dock station antennas are vertically polarized, and from the other side subset 3 is composed by eleven vertically polarized elements while subset 1 contain only four vertically polarized elements. That's why subset 3 is active not subset 1. Therefore a scenario where subset 1 could be active is when the EUT is rotated of 90 degrees (the EUT screen become in portrait mode). In this case, the subset 1 polarization ensure better link budget than subset 3. In all cases the energy will be directed away from body.

3.7.4 Case 4: EUT placed vertically with a lateral shifting to the side of the lap

Figure 13 and Figure 14 show the test results of the subset operation according to the EUT to lap distance (h), for the two horizontal distances: 45 and 90 cm respectively. The x-axis represents the height above lap while the y-axis represents, for each subset, the percentage of subset operation.

Test 1 results at 45 cm distance

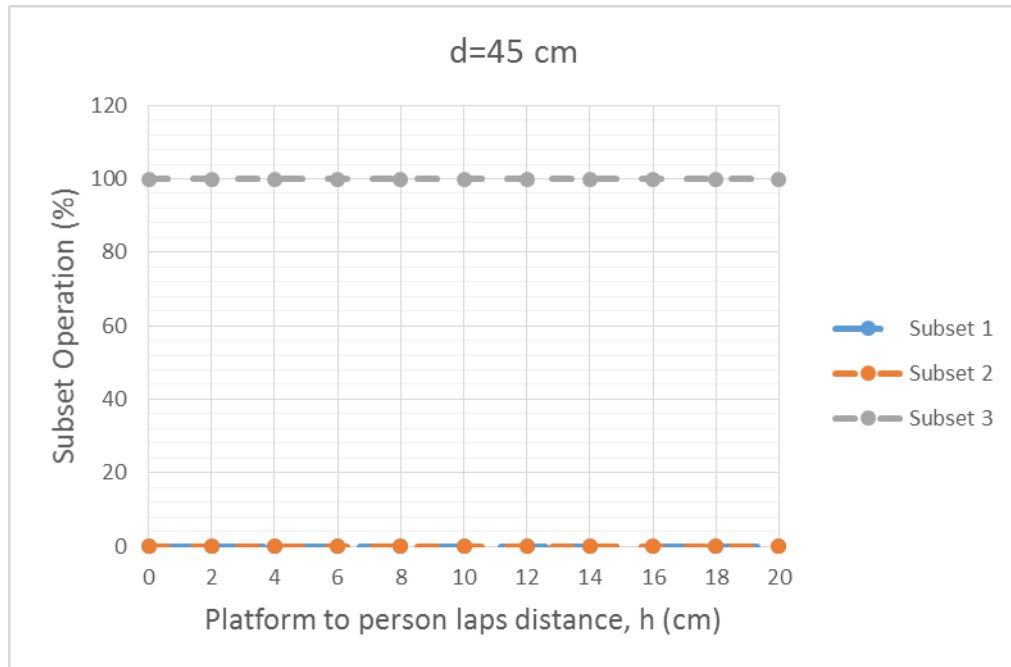


Figure 13– Percentage of subset operation at d=45 cm

Test 2 results at 90 cm distance

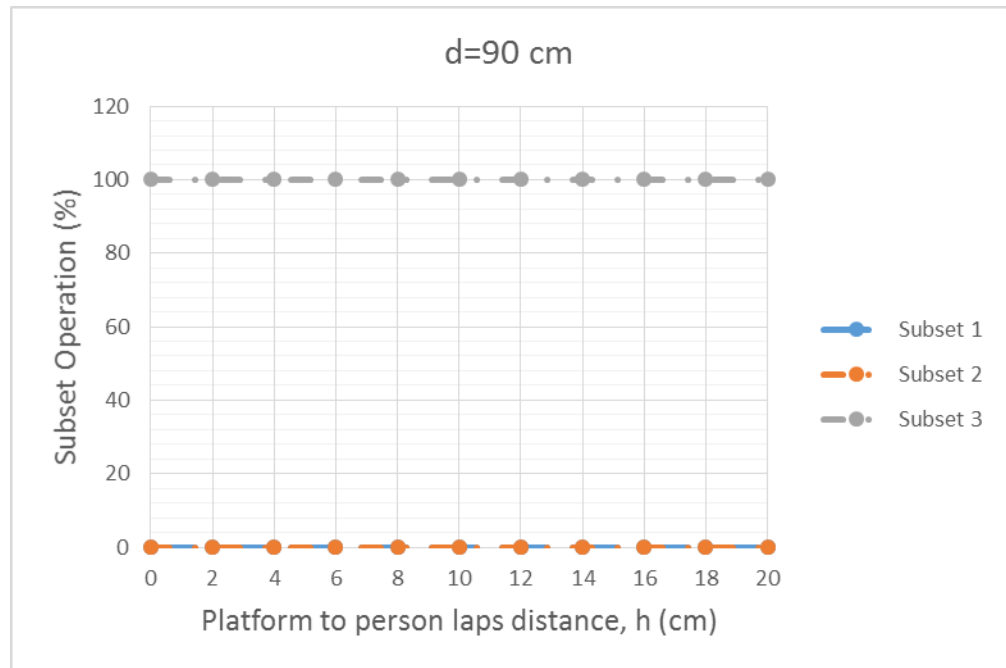


Figure 14– Percentage of subset operation at d=90 cm

Figure 13 and Figure 14 presents the results of the mitigation test when the user is holding the EUT with a lateral shifting to the side of his Lap and is placed at a distance of 45 cm and



90 cm from the Docking Station. For h going from 0 cm to 20 cm subset 3 is 100% operational among the three subsets. The transition region is not observed in this test case since the subset 3 is 100% operational for all heights.

This shows that the beam steering algorithm behaves in such a manner as to direct the energy away from the body by selecting only subset 3.

Note: In this EUT position, subset 3 is operational almost all the time rather than subset 1. This is related to a better link budget between the RFEM 3 and the dock station established by subset 3 in this EUT position. Indeed, from a side the dock station antennas are vertically polarized, and from the other side subset 3 is composed by eleven vertically polarized elements while subset 1 contain only four vertically polarized elements. That's why subset 3 is active not subset 1. Therefore a scenario where subset 1 could be active is when the EUT is rotated of 90 degrees (the EUT screen become in portrait mode). In this case, the subset 1 polarization ensure better link budget than subset 3. In all cases the energy will be directed away from body.

3.8 Conclusion

For all the measured cases when the EUT is placed horizontally on lap, with and without transverse shifting, the test results presented in Section 3.7.1 and Section 3.7.2 show that, at each horizontal distance and for all measured heights:

- When the EUT is placed close to the lap, subset 2 with a beam directed away from the body is operational almost all the time.
- When the EUT is moved forward from the lap, a transition zone is observed and a handover from subset 2 to subset 3 is done after this transition zone
- When the EUT is moved back toward the lap in reverse order, the transition zone is observed again and a switch from subset 3 to subset 2 is observed starting from the lower boundary of the transition zone.

For all the measured cases when the EUT is placed vertically on lap, with and without transverse shifting, the test results presented in section 3.7.3 and section 3.7.4 show that, at each horizontal distance and for all measured heights:

- Subset 3 with its beam directed away from the body, is operational almost all the time.

These test results confirm that the beam steering algorithm behaves in such a manner as to direct the energy away from the body while maintaining a good link budget.



Appendix A: Supplemental Numerical Modeling for RF Exposure Power Density Evaluation

A.1 Platform Simulation Methodology

A.1.1 Assessment considerations

During the system operation mode, it is challenging to define a practical system worst-case scenario in which the user is exposed to the highest emission level. To ensure coverage of the highest emission, the analysis of the worst-case condition is used and is emphasized in the following:

1. Platform orientation with respect to human body – In most of the cases, when the platform is very close to the human body, and the energy is directed to the human body, the human body will attenuate the signal. In this case, a reliable link can't be achieved. When a reliable link can't be maintained, the system enters search mode. In search mode, the system will transmit a low-duty cycle of less than 1%. This search mode contains signals which happen every 100ms at the maximum output power. However, in the analysis done for this document, the system is simulated in operational mode (not in search mode), operating at 70% duty cycle, which is much higher than the search mode.
2. Energy direction, beam forming – In order to avoid human body attenuation or object blockage of a reliable link, the system beam forming will automatically search for a path that will establish a more reliable link. So, in real life, in most of the cases the EM path will not be directed towards the human body (see Section 3). However, in the analysis presented in this document, worst-case beam forming direction is used.

Please note that the above worst-case assessment description is very conservative in that it is very unlikely that this case would happen under normal usage conditions. Since we cannot state with 100% certainty that this is impossible, we kept this worst-case assessment methodology for supplemental purposes. We ask that this be taken into consideration.

A.1.2 Near field results

Finding the worst-case emission in the near field across the platform boundary requires searching on two orthogonal domains. One domain is the location – the need to find the place that has the worst-case energy. The other domain that has to be searched is the range of antenna phases – the need to search over the various antenna phases and find the antenna phase combination that gives the worst-case value. Section A.1.4 explains how these two worst-case (location and phase) searches are investigated.

After the completion of the worst-case phase analysis, the phases found during this analysis are used to find the worst-case spatially averaged power density across a 1cm^2 , for RF exposure evaluation purposes. EM simulation is used for this analysis.

Near-field analysis is simulated and correlated against measured lab results.

A.1.3 Simulation tool

A.1.3.1 Tool description

For the EM simulation, the commercially-available ANSYS Electronics Desktop 2016 (HFSS) is used. The ANSYS HFSS tool is used in the industry for simulating 3D, full-wave electromagnetic fields. Intel uses this EM simulation tool due to its gold-standard accuracy, advanced solver, and high-performance computing technology capabilities for doing accurate and rapid design of high-frequency components.

A.1.3.2 Solver description

The HFSS simulation is performed using the Finite Element Method, which operates in the frequency domain. The HFSS is based on an accurate direct solver with first order basis functions.

A.1.3.3 Convergence criteria and power density calculations

The HFSS uses a volume air box containing the simulated area to calculate the EM fields. The box is truncated by a Perfect Match Layer (PML) boundary condition. The simulation uses the adaptive mesh technique (see Figure 15) meet the exit criteria of $\Delta S < 0.02$. The ΔS is the change in the magnitude of the S-parameters between two consecutive passes; if the magnitude and phase of all S-parameters change by an amount less than the Maximum-Delta-S-per-Pass value from one iteration to the next, the adaptive analysis stops.

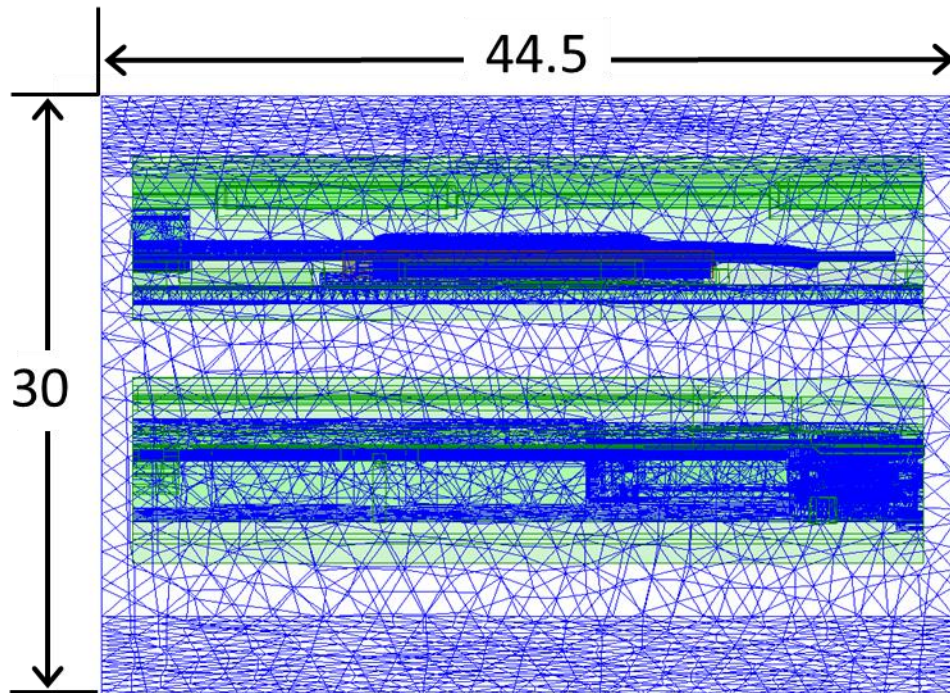


Figure 15 – Illustration of the adaptive mesh technique



After having the simulated electrical and magnetic (E and H) fields. The spatially averaged power density on a given surface is calculated as the surface integral of the Poynting vector:

$$W = \frac{1}{2} \operatorname{Re} \int_S (\vec{E} \times \vec{H}^*) \cdot \vec{n} dS$$

Notes:

1. HFSS phasors in the field calculator are peak phasors, which leads to the $1/2$ factor in the Poynting vector calculation.
2. Figure 15 is an illustration of the adaptive mesh technique and is presented in the context of simulation methodology presentation.

A.1.4 Finding the near-field, worst-case simulation configuration

As explained previously, near-field analysis requires finding the worst-case location (along the searched plane) and antenna phase values. As further explained, the search should be done on two domains:

- 1) Look for the worst-case position (across the search plane).
- 2) Look for the two worst-cases antenna phases.

Note: The search plans are defined as the plans used for the calculation of the two worst-cases antenna phase combinations. The new RFEM 3 antenna is intended to operate according to one of three predefined subsets². For each subset an evaluation plane is defined taking into account the radiation direction of this subset. As The platform Dell P29S is used exclusively in laptop mode, for all subsets, the evaluation plane corresponds to the laptop base exposure plane.

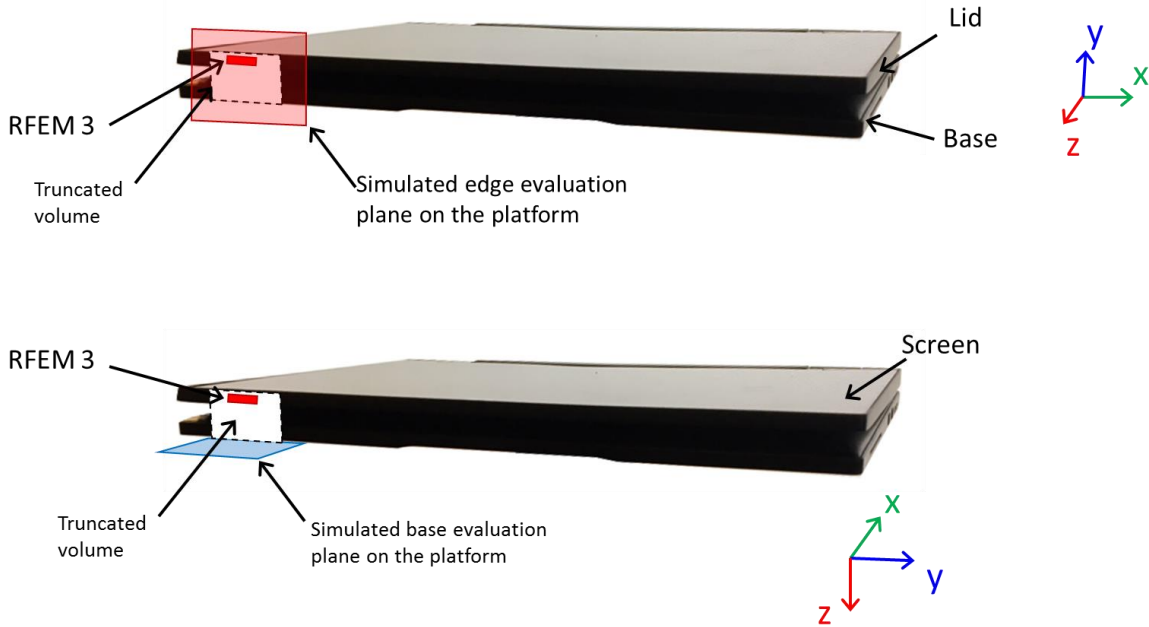


Figure 16 – The x-y search on the edge and the base evaluation planes

Note that for the xyz coordinate references used throughout this report, we always consider the z-axis as being towards the body direction. This consideration is used to conserve a general consistency for the field's representation and calculations in the worst-case determination procedure detailed below. In summary, the xy plane is the evaluation plane, and the z-axis is the vector in propagation direction towards the body.

² A subset is a group of radiating elements which are excited simultaneously with the same amplitude. In RFEM 3, the number of subsets is three.

A.1.4.1 Terminology

- Element – Each one of the radiating elements that are used in the system. We denote the antenna element with index \mathbf{k} in this explanation.
- N – Number of chains (RFEM 3 includes 24 radiated antenna elements – $\mathbf{N}=24$). As described in the previous section, there are three subsets in RFEM 3. These subsets, named subset 1, subset 2 and subset 3, are composed of 10, 11 and 11 active elements respectively. For each subset, a set of elements from the 24 radiating antennas is activated).
- Point – Each point on the grid that is used for searching for the worst- case position. They are spaced 0.1mm from each other. The grid point would be denoted as \mathbf{g} in this explanation.
- Complex E field vector generated by the \mathbf{k}^{th} antenna element at point \mathbf{g} :

$$\overrightarrow{E_{k,g}} = \vec{x}(\text{Re}[E_{kx,g}] + j\text{Im}[E_{kx,g}]) + \vec{y}(\text{Re}[E_{ky,g}] + j\text{Im}[E_{ky,g}]) + \vec{z}(\text{Re}[E_{kz,g}] + j\text{Im}[E_{kz,g}])$$
- Complex H field vector generated by the \mathbf{k}^{th} antenna element at point \mathbf{g} :

$$\overrightarrow{H_{k,g}} = \vec{x}(\text{Re}[H_{kx,g}] + j\text{Im}[H_{kx,g}]) + \vec{y}(\text{Re}[H_{ky,g}] + j\text{Im}[H_{ky,g}]) + \vec{z}(\text{Re}[H_{kz,g}] + j\text{Im}[H_{kz,g}])$$
- $\hat{x}, \hat{y}, \hat{z}$ – unit direction vectors having unit magnitude and mutually orthogonal to each other.
- Without loss of generality in this explanation, RFEM 3 and the search plane are in the \hat{x}, \hat{y} plane, and the integrated 1cm^2 plane is perpendicular to direction \hat{z} .

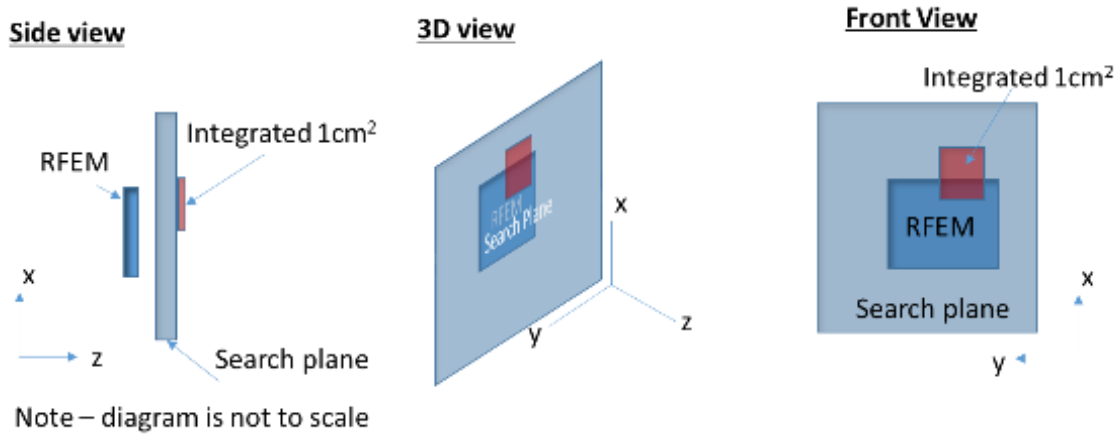


Figure 17 – Near field worst-case terminology and orientation

A.1.4.2 Primer on field vector representation

For each subset, E and H fields generated by the \mathbf{k} chain are

$$\begin{aligned}\overrightarrow{E_k} &= \vec{x}(\text{Re}[E_{kx}] + j\text{Im}[E_{kx}]) + \vec{y}(\text{Re}[E_{ky}] + j\text{Im}[E_{ky}]) + \vec{z}(\text{Re}[E_{kz}] + j\text{Im}[E_{kz}]) \\ \overrightarrow{H_k} &= \vec{x}(\text{Re}[H_{kx}] + j\text{Im}[H_{kx}]) + \vec{y}(\text{Re}[H_{ky}] + j\text{Im}[H_{ky}]) + \vec{z}(\text{Re}[H_{kz}] + j\text{Im}[H_{kz}])\end{aligned}$$

For each subset, E and H fields generated by all N chains (only subset elements are activated) are

$$\overrightarrow{E_{\text{All}}} = \vec{x} \sum_{k=1}^N (\text{Re}[E_{kx}] + j\text{Im}[E_{kx}]) + \vec{y} \sum_{k=1}^N (\text{Re}[E_{ky}] + j\text{Im}[E_{ky}]) + \vec{z} \sum_{k=1}^N (\text{Re}[E_{kz}] + j\text{Im}[E_{kz}])$$

$$\overrightarrow{H_{\text{All}}} = \vec{x} \sum_{k=1}^N (\text{Re}[H_{kx}] + j\text{Im}[H_{kx}]) + \vec{y} \sum_{k=1}^N (\text{Re}[H_{ky}] + j\text{Im}[H_{ky}]) + \vec{z} \sum_{k=1}^N (\text{Re}[H_{kz}] + j\text{Im}[H_{kz}])$$

The Poynting vector generated by all N chains is

$$\overrightarrow{P_{\text{General,All}}} = \frac{1}{2} \overrightarrow{E_{\text{All}}} \times \overrightarrow{H_{\text{All}}^*}$$

$$= \frac{1}{2} \left\{ \vec{x} \left\{ \sum_{k=1}^N (\text{Re}[E_{ky}] + j\text{Im}[E_{ky}]) \sum_{k=1}^N (\text{Re}[H_{kz}] - j\text{Im}[H_{kz}]) \right. \right.$$

$$- \sum_{k=1}^N (\text{Re}[E_{kz}] + j\text{Im}[E_{kz}]) \sum_{k=1}^N (\text{Re}[H_{ky}] - j\text{Im}[H_{ky}]) \Big\}$$

$$+ \vec{y} \left\{ \sum_{k=1}^N (\text{Re}[E_{kz}] + j\text{Im}[E_{kz}]) \sum_{k=1}^N (\text{Re}[H_{kx}] - j\text{Im}[H_{kx}]) \right. \right.$$

$$- \sum_{k=1}^N (\text{Re}[E_{kx}] + j\text{Im}[E_{kx}]) \sum_{k=1}^N (\text{Re}[H_{kz}] - j\text{Im}[H_{kz}]) \Big\}$$

$$+ \vec{z} \left\{ \sum_{k=1}^N (\text{Re}[E_{kx}] + j\text{Im}[E_{kx}]) \sum_{k=1}^N (\text{Re}[H_{ky}] - j\text{Im}[H_{ky}]) \right. \right.$$

$$- \sum_{k=1}^N (\text{Re}[E_{ky}] + j\text{Im}[E_{ky}]) \sum_{k=1}^N (\text{Re}[H_{kx}] - j\text{Im}[H_{kx}]) \Big\}$$

Power flow is

$$\text{Re}[\overrightarrow{P_{\text{General,All}}}] = \frac{1}{2} \left\{ \vec{x} \left\{ \sum_{k=1}^N \text{Re}[E_{ky}] \sum_{k=1}^N \text{Re}[H_{kz}] + \sum_{k=1}^N \text{Im}[E_{ky}] \sum_{k=1}^N \text{Im}[H_{kz}] - \sum_{k=1}^N \text{Re}[E_{kz}] \sum_{k=1}^N \text{Re}[H_{ky}] \right. \right. \right.$$

$$- \sum_{k=1}^N \text{Im}[E_{kz}] \sum_{k=1}^N \text{Im}[H_{ky}] \Big\}$$

$$+ \vec{y} \left\{ \sum_{k=1}^N \text{Re}[E_{kz}] \sum_{k=1}^N \text{Re}[H_{kx}] + \sum_{k=1}^N \text{Im}[E_{kz}] \sum_{k=1}^N \text{Im}[H_{kx}] - \sum_{k=1}^N \text{Re}[E_{kx}] \sum_{k=1}^N \text{Re}[H_{kz}] \right. \right. \right.$$

$$- \sum_{k=1}^N \text{Im}[E_{kx}] \sum_{k=1}^N \text{Im}[H_{kz}] \Big\}$$

$$+ \vec{z} \left\{ \sum_{k=1}^N \text{Re}[E_{kx}] \sum_{k=1}^N \text{Re}[H_{ky}] + \sum_{k=1}^N \text{Im}[E_{kx}] \sum_{k=1}^N \text{Im}[H_{ky}] - \sum_{k=1}^N \text{Re}[E_{ky}] \sum_{k=1}^N \text{Re}[H_{kx}] \right. \right. \right.$$

$$- \sum_{k=1}^N \text{Im}[E_{ky}] \sum_{k=1}^N \text{Im}[H_{kx}] \Big\}$$

A.1.4.3 Domain search for worst-case direction

The two domain search is completed (for each subset) as follows:

- A. First find a direction (location) for the worst-case 1cm² square averaging area using upper-bound methods.

The basic concept behind the upper-bound method is to assume that there could be an “ideal beam forming” mechanism that could align the phases of all the elements for both E and H fields. (Obviously, in real life this cannot happen. This is the reason that this is an upper-bound method). When this ideal mechanism is used, then all the complex phasors are aligned to the same phase, hence the phasor absolute value can be used instead of the phasor. The E (and H) field for any direction is the sum of the magnitude of the fields (look at item 3, below, for a more formal description).

This method provides the worst-case position independent of the antenna phases. It allows finding the worst-case location with this “ideal beam forming” mechanism.

Item 3, below, translates the above verbal description into more formal mathematical wording.

- B. After the worst-case direction is found using the upper-bound method for each subset, the antenna phases are aligned to this direction. The antenna phases are aligned to maximize the power across the 1cm² averaging area that was found using the upper-bound method. The method that is used to find the required antenna phases is as follows: first order the antennas of the subset according to the power contribution on the found 1cm² from the highest to the lowest. Then start by activating the antenna that contributes the most, set its phase to 0, and then activate the 2nd antenna and search over the phases for the 2nd antenna. Choose the phase that maximizes the power of the two antenna elements. To find the phase for the third antenna, fix antenna 1’s phase to zero and antenna 2’s phase to the value that was found before. Then search for the phases for the third antenna that maximize the power. Continue with the same process until you reach the last subset element. The same process is used to find the second worst case.
- C. Calculate the power density with the antenna phases that were found in the previous item (item B).

The above process can be written as the following algorithm:

1. A grid is defined with 0.1mm spacing.
2. At each point in the grid, the complex E and H fields are calculated using each one of all radiating elements in the involved subset, separately. Each one of the calculated E and H fields are 3D complex vectors, so the simulation output from this stage is 10, 11, 11 3D complex E field strength vectors and 10, 11, 11 3D complex H field strength vectors for the three subsets respectively . The vectors are defined as:

$$\overrightarrow{E_{k,g}} = \vec{x}(\operatorname{Re}[E_{kx,g}] + j\operatorname{Im}[E_{kx,g}]) + \vec{y}(\operatorname{Re}[E_{ky,g}] + j\operatorname{Im}[E_{ky,g}]) + \vec{z}(\operatorname{Re}[E_{kz,g}] + j\operatorname{Im}[E_{kz,g}]) \text{ and}$$

$$\overrightarrow{H_{k,g}} = \vec{x}(\operatorname{Re}[H_{kx,g}] + j\operatorname{Im}[H_{kx,g}]) + \vec{y}(\operatorname{Re}[H_{ky,g}] + j\operatorname{Im}[H_{ky,g}]) + \vec{z}(\operatorname{Re}[H_{kz,g}] + j\operatorname{Im}[H_{kz,g}])$$

3. Upper-bound assumption is used to derive the E and H field on each one of the grid points. The following items describe the upper-bound method that is used:
 - a. The calculation is made separately for E field and H field.

- b. For E field, the following calculation is made independently for each one of the grid points:

$$\overrightarrow{E_{UB,g}} = \vec{x} \sum_{k=1}^N \sqrt{\operatorname{Re}[E_{kx,g}]^2 + \operatorname{Im}[E_{kx,g}]^2} + \vec{y} \sum_{k=1}^N \sqrt{\operatorname{Re}[E_{ky,g}]^2 + \operatorname{Im}[E_{ky,g}]^2} \\ + \vec{z} \sum_{k=1}^N \sqrt{\operatorname{Re}[E_{kz,g}]^2 + \operatorname{Im}[E_{kz,g}]^2} = \vec{x} \sum_{k=1}^N |E_{kx}| + \vec{y} \sum_{k=1}^N |E_{ky}| + \vec{z} \sum_{k=1}^N |E_{kz}|$$

The magnitude of the complex E vector is summed over the antenna elements in a subset. The summation is done for each one of the grid points, and for each one of the elements in each direction, independently.

- c. The output of the previous item is the 3D real vector of the E field on each one of the simulated grid points in each direction. The physical implementation is that an ideal beam forming was done for the E field for each one of the points.
- d. The same process as described in item b is done for the H field.

$$\overrightarrow{H_{UB,g}} = \vec{x} \sum_{k=1}^N \sqrt{\operatorname{Re}[H_{kx,g}]^2 + \operatorname{Im}[H_{kx,g}]^2} + \vec{y} \sum_{k=1}^N \sqrt{\operatorname{Re}[H_{ky,g}]^2 + \operatorname{Im}[H_{ky,g}]^2} \\ + \vec{z} \sum_{k=1}^N \sqrt{\operatorname{Re}[H_{kz,g}]^2 + \operatorname{Im}[H_{kz,g}]^2} = \vec{x} \sum_{k=1}^N |H_{kx,g}| + \vec{y} \sum_{k=1}^N |H_{ky,g}| + \vec{z} \sum_{k=1}^N |H_{kz,g}|$$

- e. At each point in the grid, the Poynting vector is calculated by vector multiplication of the E and H fields, which are added up in items b and d. As explained before, without a loss of generality, we assume that the search plane is the x/y plane. All three (xyz) components of the Poynting vector are added, and not just the component that is normal to the x/y plane:

$$P_g = \frac{1}{2} \operatorname{Re}\{(\vec{E} \times \vec{H}^*)\} = \frac{1}{2} \operatorname{Re}\{\left(((E_y H_z^* - E_z H_y^*) \hat{x} + ((E_z H_x^* - E_x H_z^*) \hat{y} + (E_x H_y^* - E_y H_x^*) \hat{z}) \right)\} \\ P_{g,x} = \frac{1}{2} \operatorname{Re}\{E_y H_z^* - E_z H_y^*\} \\ P_{g,y} = \frac{1}{2} \operatorname{Re}\{(E_z H_x^* - E_x H_z^*)\} \\ P_{g,z} = \frac{1}{2} \operatorname{Re}\{E_x H_y^* - E_y H_x^*\} \\ PUpperBound_g = \sqrt{P_{g,x}^2 + P_{g,y}^2 + P_{g,z}^2}$$

- 4. The above calculated Poynting vectors are used to estimate the power across 1cm² area.

$$P1cm2 = \iint_{1cm^2} PUpperBound_g x,y,z$$

- 5. The 1cm² area with the highest power value is used as the worst-case direction of a subset. The antenna phases are aligned to maximize the energy in this 1cm² area, as explained below in order to find the 2 worst cases:



- a. Turn on each element one-by-one to find order of power intensity in the 1cm² window. (Find the order of contribution)
- b. Sort in the power order from the highest to the lowest, #0 to #(10, 11, 11) for the involved subsets 1,2 and 3 respectively .
- c. Turn on #0 with phase P0=0. (reference)
- d. Turn on #1 and change the phase to maximize the power and find the phase P1.
- e. Keep P0 and P1 on, then turn on #2 and do same.
- f. Repeat for the rest of the antennas.

6. Using the antenna phases that were calculated in step 5, the power density is calculated along the evaluation plane and then spatially averaged across a 1cm² area.

A.1.5 3D models used in the simulation

A.1.5.1 Worst-case operating conditions of the platform

The Dell model P29S is a platform with the ability to rotate the screen by 360°. This ability allows the platform to work in various operation mode (e.g. laptop mode, tablet mode...). The worst case condition regarding the radiated near field was found for tablet operating mode. When tablet operating mode is set, the lid is rotated by 360 where the screen is folded over on top of the keyboard.

The worst-case exposition to radio frequency radiation can happen when the body of the user is in contact with the platform. The two evaluation planes illustrated in the Figure 18 represent the worst case condition in the platform configured in tablet mode:

- **Edge:** The human body is adjacent to platform edge – this mode represents the case in which a person is holding the platform in their hand and the platform edge touching their body. In this scenario the worst case emission is searched along the edge evaluation plane.
- **Base:** The human body is below the base (keyboard) – this mode represents the case in which a person holds the platform like a regular tablet and places the platform on their lap. In this scenario the worst case emission is searched along the base evaluation plane.

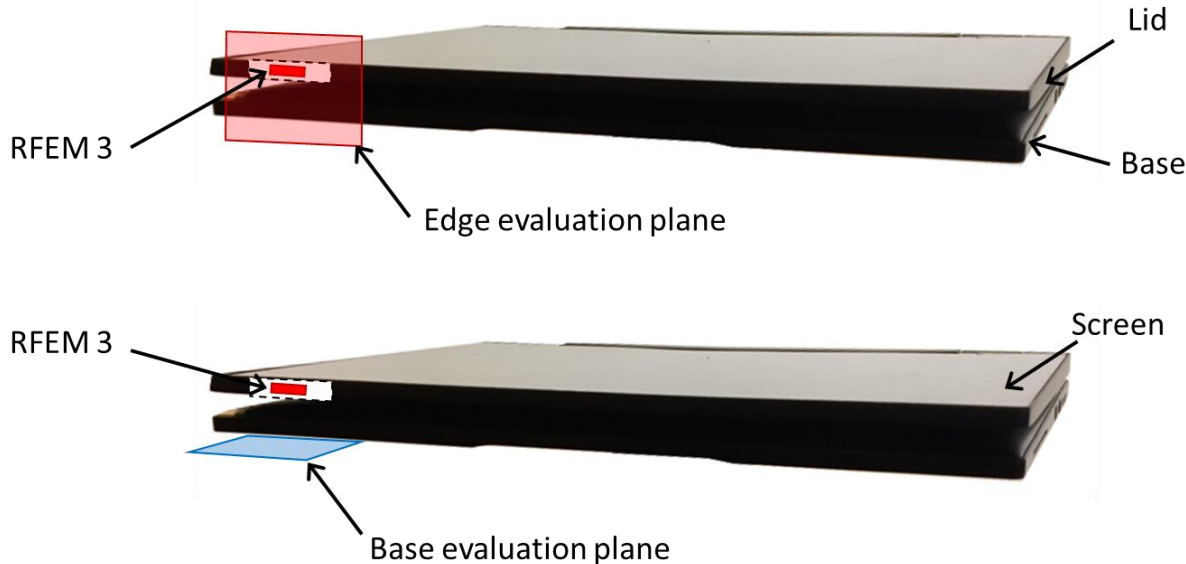


Figure 18 – Worst-case evaluation plane for Dell model P29S platform

A.1.5.2 RFEM 3 housing inside Intel 18265NGW module

The 3D Intel 18265NGW module is simulated inside the Dell P29S platform. Figure 19 shows the position of the RFEM 3 antenna, which is located inside the lid at the bottom right of the screen.



Figure 19 – Platform picture with RFEM 3 location

A.1.5.3 Closest distance to the body of an end user

In tablet operating mode, two cases were analyzed:

1. The human body is adjacent to platform edge – this mode represents the case in which a person is holding the platform in their hand and the platform edge touching their body. In this scenario the worst case emission is searched along the edge plane (showed in red in Figure 18) and the distance between human body to the active antenna is 3.25 mm.
2. The human body is below the base (keyboard) – this mode represents the case in which a person holds the platform like a regular tablet and places the platform on their lap. In this scenario, the worst case emission is searched along the base plane (showed in blue in Figure 18) and the distance between the human body to the active antenna is 16 mm.

Figure 20 shows also a cross-section (in the yz-plane) of the bottom of the lid with the RFEM 3 inside the platform.

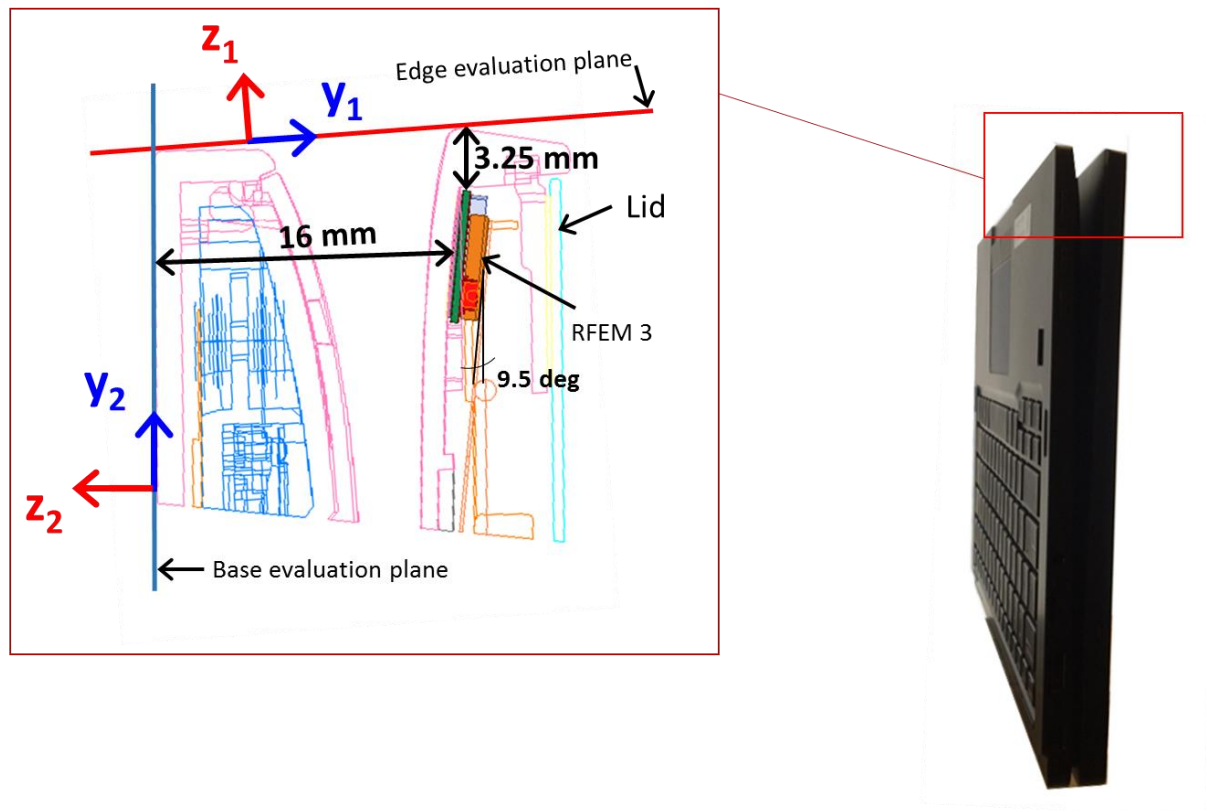


Figure 20 – Platform evaluation planes touching the body



A.1.5.4 Metals in proximity of the RFEM 3

All the metals that are in the RFEM 3 region (12.6 mm on each side) were included in the simulation.



A.1.6 Antenna feed

This section provides a general description of the numerical simulations; other details of the simulation geometry are included in reference [1]. The EM simulation uses an accurate 3D model of the RFEM 3 antenna. The model includes the antenna elements as well as their feeding lines.

In the simulation (as well as in the product), each antenna element is fed independently, and we excite the antennas at the origin of the antenna structure on the RFEM 3. (The antenna structure includes the silicon chip, the solder bumps, the vias, traces and actual antenna element.)

As described previously, the RFEM 3 antenna will be operated according to one of three predefined subsets. For the operational subset, signals of equal amplitude are applied to the feed-points of individual array elements, and the aggregate equivalent conducted power to all array elements corresponds to the sum of all elements' powers. In the worst-case power density the subset 1 is the operational subset with an equivalent conducted power of 6.5 dBm; thus each element is fed by -3.5 dBm (6.5 dBm divided over 10 elements).

The total power (same per element) is used to build the pattern of radiated power through beam forming. For building the beam forming pattern, the same power is used per element, while phase is changed per element. (Refer to Section 2.2 for more information about beam forming). Phases are derived for each excitation separately, to simulate the worst-case condition. Section A.1.4 explains how the phases are derived to find the worst case condition.

A.2 Power Density Simulation Results

A.2.1 Introduction

The evaluation planes presented in Section A.1.5.2 has been simulated according to the methodology described in Section A.1. The simulation results for all subsets in the concerned evaluation planes are presented in this section.

The power density has been simulated over three channels with frequencies listed in Table 4. For each channel, we'll present the resulting details according to the methodology explained in Section A.1.4:

- Simulation results of the upper bound single-point power density for each single-point across the mesh ($P_{UpperBound_g}$). Please note that this value represents single-point power density and not spatially averaged power density over 1cm^2 . Even though a 1mW/cm^2 scale is used, this value represents an upper-bound power density for each single point of the mesh, which is a much smaller area than 1cm^2 .
- The results of the single-point power density using the antenna phases corresponding to the first and second worst-cases.
- Spatially averaged power density over 1cm^2 results of the first and second worst-case for each subset antenna phases. These results present the spatially averaged power density across 1cm^2 using the xyz components of the Poynting vector.
- All results for all channels and subsets are normalized to the target maximum power of 6.5 dBm

Table 4 – WiGig channel frequencies

| | Channel 1 | Channel 2 | Channel 3 |
|-----------------|-----------|-----------|-----------|
| Frequency (GHz) | 58.32 | 60.48 | 62.64 |

Table 5 summarizes all the simulation configurations as well as the result types presented in this section:

Table 5 – Power density simulation configuration and result details

| Subset | Evaluation Planes | Channels | Results types | Count | Reference |
|------------|-------------------|-------------|---|--|-----------------|
| 1, 2 and 3 | Edge plane | 1, 2, and 3 | Upper-bound power density | 3 channels x 3 Subsets | Table 6 |
| | | | 1 st worst-case antenna phases | 3 channels x 3 Subsets | Table 7 |
| | | | 2 nd worst-case antenna phases | 3 channels x 3 Subsets | Table 8 |
| | | | single point power density | 2 Worst cases x 3 channels x 3 Subsets | Table 9 |
| | | | spatially averaged power density | 2 Worst cases x 3 channels x 3 Subsets | Table 10 |
| | | Base plane | Worst-case distribution ⁽¹⁾ | [3 plots] – Very worst case | Section A.2.2.5 |
| | | | Upper-bound power density | 3 channels x 3 Subsets | Table 12 |
| | | | 1 st worst-case antenna phases | 3 channels x 3 Subsets | Table 13 |
| | | | 2 nd worst-case antenna phases | 3 channels x 3 Subsets | Table 14 |
| | | | single point power density | 2 Worst cases x 3 channels x 3 Subsets | Table 15 |
| | | | spatially averaged power density | 2 Worst cases x 3 channels x 3 Subsets | Table 16 |
| | | | Worst-case distribution ⁽¹⁾ | [3 plots] – Very worst case | A.2.3.5 |

⁽¹⁾ The distribution of the found worst case spatially averaged power density among the 18 calculated worst cases.

A.2.2 Simulation Results on the edge evaluation plane

A.2.2.1 Upper bound power density values in the edge evaluation plane

The Upper Bound single-point power density is calculated for each subset of the antenna. Table 6 summarizes, for all subsets, the maximum calculated upper bound single point power density.

Please note that since the worst-case conditions are searched over a plane for near field, then the azimuth and the elevation are not relevant. The worst-case position is calculated using all the power density single-points issued from the upper-bound simulation results. We leverage the phase conditions for each antenna element that resulted in these worst-case conditions to evaluate final spatially averaged power density. The mathematical basis for using these as the worst-case phase conditions to evaluate the final spatially averaged power density were provided in Section A.1.4.3.

Table 6 – Maximum upper bound single point power density [mW/cm²]

| | Channel 1 | Channel 2 | Channel 3 |
|----------|-----------|-----------|-----------|
| Subset 1 | 11.812 | 13.168 | 11.161 |
| Subset 2 | 17.946 | 20.707 | 19.023 |
| Subset 3 | 14.068 | 13.373 | 11.749 |



A.2.2.2 Worst-case antenna phases in the edge evaluation plane

The phase's configurations a.k.a. 'beamforming codes' for the first and second worst power density cases are calculated for each subset and each channel using the phase search algorithm detailed in bullet 5 of Section A.1.4.3.

Table 7 and Table 8 shows, for each channel, the phases of each subset elements (marked in grey) in the first and second worst power density case respectively. The white cells with phase ("–") correspond to the non-active elements of the subset. For instance, for subset 1, the active elements are 7, 8; 17 to 24 and the worst case occurs for each channel with the indicated phases. "Ph #" indicates the number of the attributed phase combination for each worst case.

**Table 7 –Phases configurations for the first worst case for all antenna subsets**

| Antenna index | Subset 1 – Base plane Phases [Degrees] | | | Subset 2 –Base plane Phases [Degrees] | | | Subset 3 – Base plane Phases [Degrees] | | |
|---------------|--|-------|-------|---------------------------------------|-------|-------|--|-------|-------|
| | CH1 | CH2 | CH3 | CH1 | CH2 | CH3 | CH1 | CH2 | CH3 |
| | Ph #1 | Ph #2 | Ph #3 | Ph #4 | Ph #5 | Ph #6 | Ph #7 | Ph #8 | Ph #9 |
| 1 | - | - | - | - | - | - | 180 | 180 | 90 |
| 2 | - | - | - | - | - | - | 0 | 0 | 90 |
| 3 | - | - | - | - | - | - | 0 | 0 | 0 |
| 4 | - | - | - | 270 | 270 | 270 | - | - | - |
| 5 | - | - | - | 0 | 0 | 0 | - | - | - |
| 6 | - | - | - | 270 | 270 | 270 | - | - | - |
| 7 | 180 | 180 | 180 | - | - | - | - | - | - |
| 8 | 180 | 180 | 180 | - | - | - | - | - | - |
| 9 | - | - | - | 0 | 90 | 90 | - | - | - |
| 10 | - | - | - | 90 | 180 | 270 | - | - | - |
| 11 | - | - | - | 180 | 270 | 270 | - | - | - |
| 12 | - | - | - | 270 | 270 | 0 | - | - | - |
| 13 | - | - | - | 90 | 0 | 90 | 270 | 270 | 180 |
| 14 | - | - | - | 180 | 90 | 180 | 270 | 270 | 270 |
| 15 | - | - | - | 180 | 90 | 180 | 270 | 270 | 270 |
| 16 | - | - | - | 0 | 270 | 0 | 270 | 270 | 0 |
| 17 | 90 | 90 | 270 | - | - | - | - | - | - |
| 18 | 180 | 180 | 180 | - | - | - | - | - | - |
| 19 | 180 | 180 | 180 | - | - | - | - | - | - |
| 20 | 0 | 0 | 0 | - | - | - | - | - | - |
| 21 | 90 | 270 | 270 | - | - | - | 270 | 270 | 0 |
| 22 | 180 | 90 | 90 | - | - | - | 0 | 0 | 180 |
| 23 | 180 | 90 | 90 | - | - | - | 0 | 0 | 180 |
| 24 | 0 | 270 | 270 | - | - | - | 180 | 180 | 0 |

**Table 8 –Phases configurations for the second worst case for all antenna subsets**

| Antenna index | Subset 1 – Base plane Phases [Degrees] | | | Subset 2 –Base plane Phases [Degrees] | | | Subset 3 – Base plane Phases [Degrees] | | |
|---------------|--|--------|--------|---------------------------------------|--------|--------|--|--------|--------|
| | CH1 | CH2 | CH3 | CH1 | CH2 | CH3 | CH1 | CH2 | CH3 |
| | Ph #10 | Ph #11 | Ph #12 | Ph #13 | Ph #14 | Ph #15 | Ph #16 | Ph #17 | Ph #18 |
| 1 | - | - | - | - | - | - | 180 | 180 | 180 |
| 2 | - | - | - | - | - | - | 0 | 90 | 0 |
| 3 | - | - | - | - | - | - | 0 | 0 | 0 |
| 4 | - | - | - | 270 | 270 | 0 | - | - | - |
| 5 | - | - | - | 0 | 0 | 0 | - | - | - |
| 6 | - | - | - | 180 | 0 | 270 | - | - | - |
| 7 | 90 | 180 | 180 | - | - | - | - | - | - |
| 8 | 0 | 90 | 180 | - | - | - | - | - | - |
| 9 | - | - | - | 270 | 90 | 90 | - | - | - |
| 10 | - | - | - | 90 | 270 | 0 | - | - | - |
| 11 | - | - | - | 180 | 0 | 270 | - | - | - |
| 12 | - | - | - | 180 | 90 | 0 | - | - | - |
| 13 | - | - | - | 270 | 270 | 180 | 270 | 270 | 180 |
| 14 | - | - | - | 90 | 0 | 180 | 270 | 0 | 270 |
| 15 | - | - | - | 270 | 270 | 270 | 270 | 270 | 270 |
| 16 | - | - | - | 90 | 90 | 90 | 270 | 0 | 90 |
| 17 | 90 | 90 | 270 | - | - | - | - | - | - |
| 18 | 180 | 90 | 90 | - | - | - | - | - | - |
| 19 | 180 | 90 | 90 | - | - | - | - | - | - |
| 20 | 0 | 0 | 0 | - | - | - | - | - | - |
| 21 | 0 | 270 | 270 | - | - | - | 270 | 270 | 270 |
| 22 | 90 | 90 | 90 | - | - | - | 0 | 90 | 90 |
| 23 | 0 | 90 | 90 | - | - | - | 0 | 90 | 180 |
| 24 | 270 | 270 | 270 | - | - | - | 180 | 270 | 270 |



A.2.2.3 Single-Point power density values in the edge evaluation plane

Table 9 presents, for all channels and subsets, the calculated single-point power density values in the concerned evaluation plane using the first and the second worst-case subset antenna phases presented in Table 7 and Table 8 respectively (18 Worst cases).

Table 9 – Maximum single point power density [mW/cm²]

| | First worst case | | | Second worst case | | |
|-----------------|------------------|-----------|-----------|-------------------|-----------|-----------|
| | Channel 1 | Channel 2 | Channel 3 | Channel 1 | Channel 2 | Channel 3 |
| Subset 1 | 2.783 | 3.095 | 1.715 | 2.1504 | 2.7405 | 1.5189 |
| Subset 2 | 2.237 | 1.940 | 2.208 | 1.5356 | 3.3597 | 1.8511 |
| Subset 3 | 2.590 | 2.0741 | 2.6389 | 2.5896 | 2.531 | 1.999 |

A.2.2.4 Spatially averaged power density over 1 cm² values in the evaluation plane

Table 10 shows, for all channels and subsets, the calculated spatially averaged power density over 1 cm² at 100% duty cycle (Eighteen Calculated worst cases). These values are calculated in the concerned evaluation plane using the first and the second worst-case subset antenna phases shown in Table 7 and Table 8 respectively. The 6 highest spatially averaged power density are marked in bold in Table 11. Simulated field and power density distributions at the evaluation plane are provided for the six configurations in Section A.2.7.

Table 10 – Maximum spatially averaged power density over 1cm² [mW/cm²]

| | First worst case | | | Second worst case | | |
|----------|------------------|--------------|--------------|-------------------|--------------|-----------|
| | Channel 1 | Channel 2 | Channel 3 | Channel 1 | Channel 2 | Channel 3 |
| Subset 1 | 0.821 | 0.737 | 0.491 | 0.772 | 0.675 | 0.488 |
| Subset 2 | 0.612 | 0.700 | 0.712 | 0.527 | 0.672 | 0.670 |
| Subset 3 | 0.657 | 0.663 | 0.492 | 0.654 | 0.631 | 0.487 |

Table 10 shows that the very worst case is found for **subset 1 at channel 1** (marked in orange) with spatially averaged power density of **0.824 mW/cm²** at 100 % duty cycle. The next section presents all power density distributions for this worst cases.

A.2.2.5 Worst case power density distribution

As described in the previous section, the worst case spatially averaged power density over 1 cm² among the eighteen calculated worst-cases is found for subset 1, channel 1. The worst case subset antenna phase's configuration used in this case is for the first worst case (see Table 7, subset 1 / channel 1 configuration).

This section present for this worst case the distribution of the following listed items:

- Upper bound single point power density distribution
- Single-point power density distribution
- One dimensional cut of the single-point power density distribution
- Spatially averaged power density over 1 cm²

Upper-bound power density distribution

Figure 21 presents upper-bound, single-point power density of subset 1, channel 1 which is the worst case among the two simulated worst cases of the three subsets. The evaluation plane of subset 1 is the base plane represented in Figure 17.

The footprint of the platform components in the base evaluation plane for single-point power density representation is shown in Figure 23.

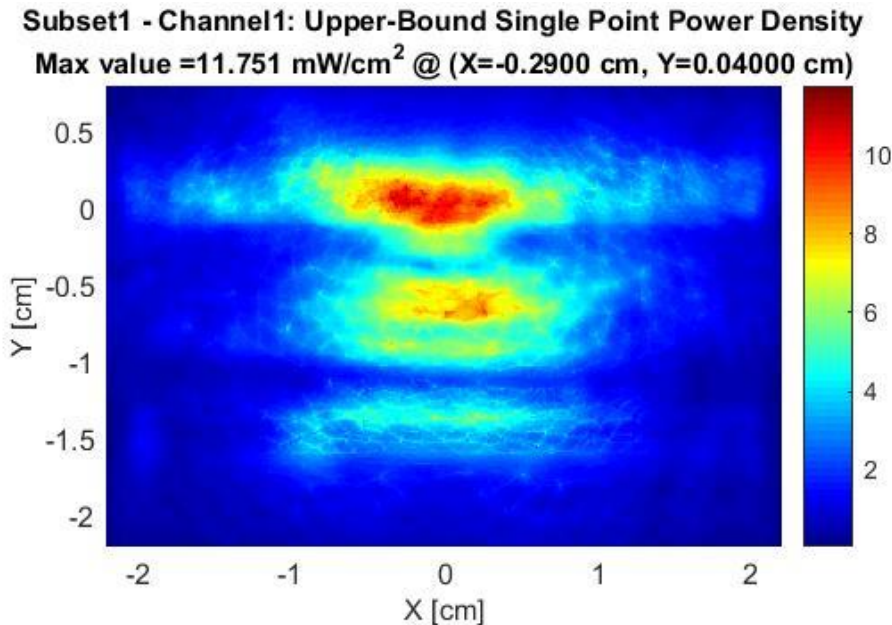


Figure 21 – Channel 1 upper-bound, single-point power density- subset 1

Single point power density distribution

Figure 22 presents the single-point power density distribution of subset 1, channel 1 in the base plane using the worst-case antenna phases of subset 1 (see Table 7)

The footprint of the platform components in the base plane for single-point power density representation is shown in Figure 23.

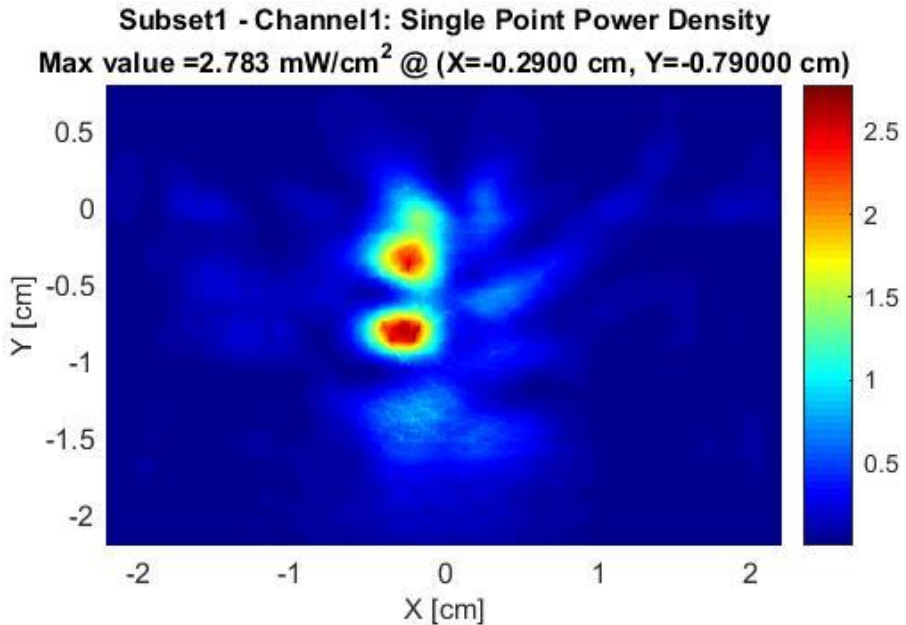


Figure 22 – Channel 1 single-point power density - subset 1

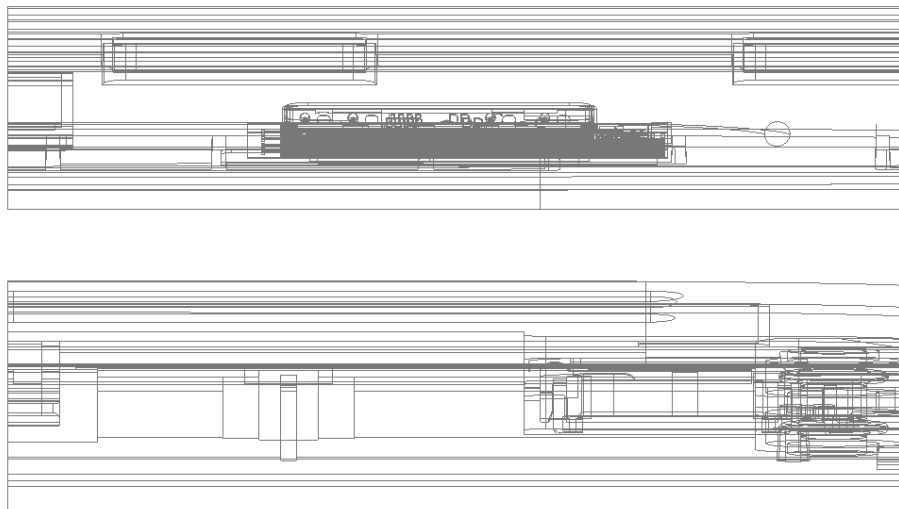


Figure 23 – Footprint of single-point power density plane representation

One dimensional cut of the single-point power density distribution

In Figure 24 and Figure 25, we present the simulation results from the xyz components of single-point power density values with worst-case antenna phases of subset 1, channel 1 which is the worst case among the three subsets. The figures represent a 1-dimensional cut in the x-axis and y-axis that shows the behavior of the near field power density at the evaluation plane.

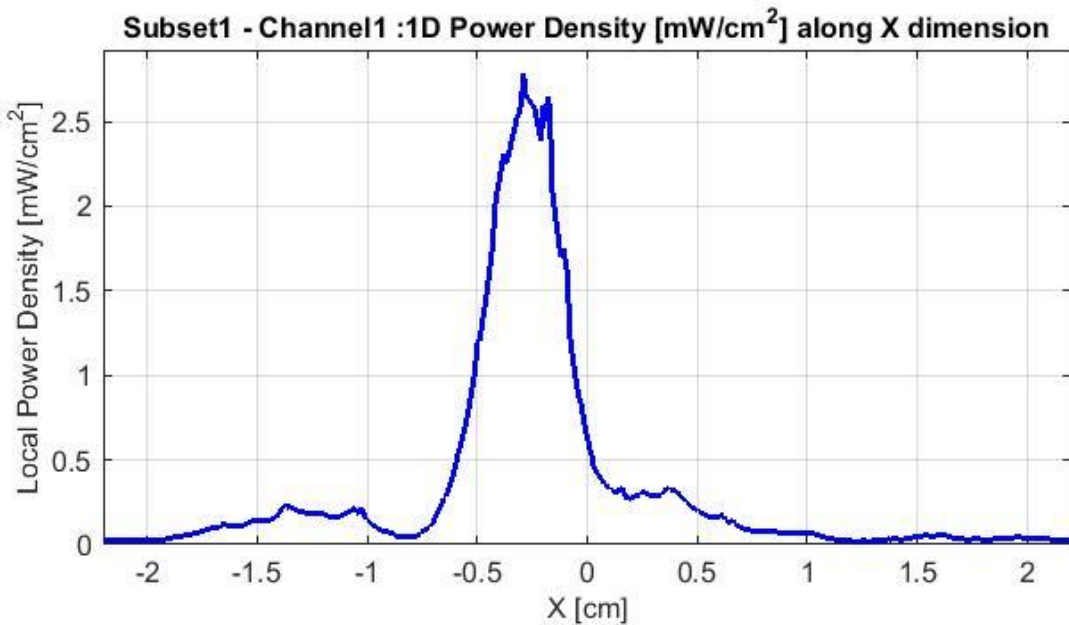


Figure 24 – 1-dimensional plots of the power density along x dimension

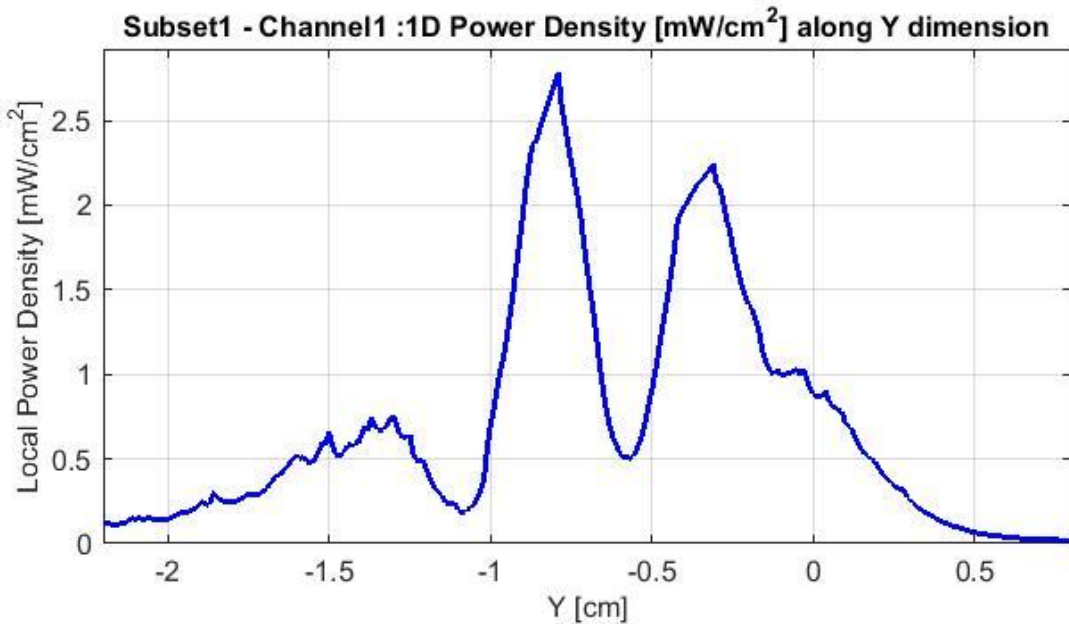


Figure 25 – 1-dimensional plots of the power density along y dimension

Distribution of Spatially averaged power density over 1 cm²

Figure 26 presents the spatially averaged power over 1cm² at 100% duty cycle for the worst-case scenario of subset 1, channel 1 as explained in Section A.1.4.3.

The 1cm² square location correspondent to the maximum of spatially averaged power density value is plotted in Figure 26 for the channel 1.

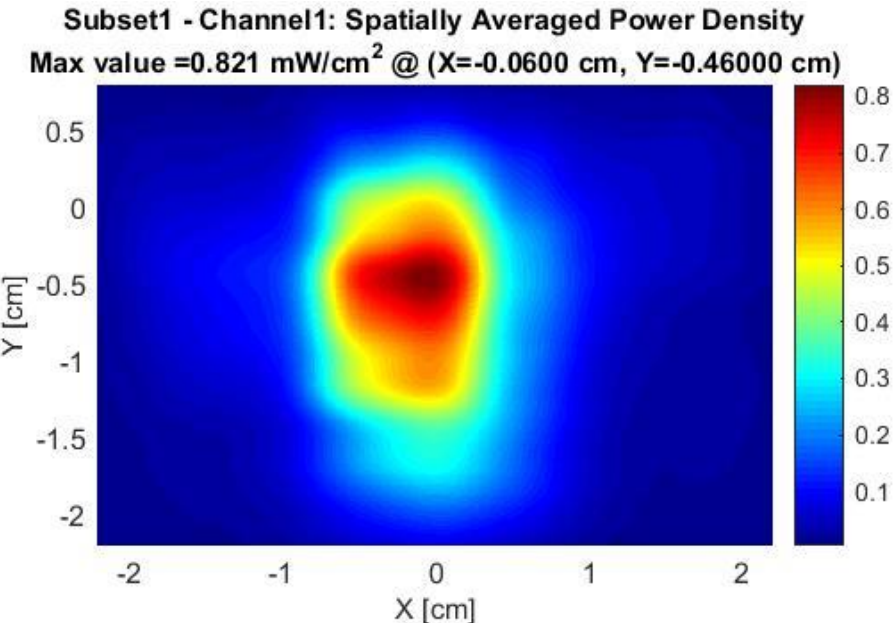


Figure 26 – Channel 1– spatially averaged power density over 1cm2 – subset 1

The Table 11 shows the simulated worst-case power density, for subset 1 – channel 1, in the evaluation plane.

Table 11 – Worst-case power density – Subset 1

| Highest power density | Subset 1 - Channel 1 |
|-----------------------|----------------------|
| 70% duty cycle | 0.576 |
| 100% duty cycle | 0.824 |

Notes for Table 11

1. The worst-case power density is found for channel 1 on subset 1.
2. The Maximum power density (spatially averaged over worst 1cm²) in channel 1 is achieved at 0 mm distance from the platform boundary and equals 0.824mW/cm² over 100% duty cycle.
3. As explained in Section 2.4, the Intel 18265NGW module is limited to transmit at a duty cycle of 70% over 10 seconds. Therefore the maximum spatially-integrated and time-averaged power density over 1cm² is 0.824x 0.7 = 0.576 mW/cm².

A.2.3 Simulation Results on the base evaluation plane

A.2.3.1 Upper bound power density values in the base evaluation plane

The Upper Bound single-point power density is calculated for each subset of the antenna. Table 12 summarizes, for all subsets, the maximum calculated upper bound single point power density.

Please note that since the worst-case conditions are searched over a plane for near field, then the azimuth and the elevation are not relevant. The worst-case position is calculated using all the power density single-points issued from the upper-bound simulation results. We leverage the phase conditions for each antenna element that resulted in these worst-case conditions to evaluate final spatially averaged power density. The mathematical basis for using these as the worst-case phase conditions to evaluate the final spatially averaged power density were provided in Section A.1.4.3.

Table 12 – Maximum upper bound single point power density [mW/cm²]

| | Channel 1 | Channel 2 | Channel 3 |
|----------|-----------|-----------|-----------|
| Subset 1 | 5.300 | 3.966 | 2.344 |
| Subset 2 | 1.453 | 1.475 | 1.568 |
| Subset 3 | 6.682 | 6.076 | 3.576 |

A.2.3.2 Worst-case antenna phases in the base evaluation plane

The phase's configurations a.k.a. 'beamforming codes' for the first and second worst power density cases are calculated for each subset and each channel using the phase search algorithm detailed in bullet 5 of Section A.1.4.3.

Table 13 and Table 14 shows, for each channel, the phases of each subset elements (marked in grey) in the first and second worst power density case respectively. The white cells with phase ("–") correspond to the non-active elements of the subset. For instance, for subset 1, the active elements are 7, 8; 17 to 24 and the worst case occurs for each channel with the indicated phases. "Ph #" indicates the number of the attributed phase combination for each worst case.

**Table 13 –Phases configurations for the first worst case for all antenna subsets**

| Antenna index | Subset 1 – Base plane Phases [Degrees] | | | Subset 2 – Base plane Phases [Degrees] | | | Subset 3 – Base plane Phases [Degrees] | | |
|---------------|--|-------|-------|--|-------|-------|--|-------|-------|
| | CH1 | CH2 | CH3 | CH1 | CH2 | CH3 | CH1 | CH2 | CH3 |
| | Ph #1 | Ph #2 | Ph #3 | Ph #4 | Ph #5 | Ph #6 | Ph #7 | Ph #8 | Ph #9 |
| 1 | - | - | - | - | - | - | 180 | 90 | 0 |
| 2 | - | - | - | - | - | - | 0 | 0 | 270 |
| 3 | - | - | - | - | - | - | 0 | 0 | 270 |
| 4 | - | - | - | 0 | 0 | 270 | - | - | - |
| 5 | - | - | - | 180 | 90 | 0 | - | - | - |
| 6 | - | - | - | 180 | 0 | 0 | - | - | - |
| 7 | 180 | 180 | 180 | - | - | - | - | - | - |
| 8 | 180 | 180 | 270 | - | - | - | - | - | - |
| 9 | - | - | - | 0 | 0 | 270 | - | - | - |
| 10 | - | - | - | 90 | 90 | 0 | - | - | - |
| 11 | - | - | - | 0 | 90 | 0 | - | - | - |
| 12 | - | - | - | 90 | 180 | 90 | - | - | - |
| 13 | - | - | - | 0 | 270 | 90 | 180 | 180 | 0 |
| 14 | - | - | - | 180 | 90 | 0 | 0 | 0 | 270 |
| 15 | - | - | - | 0 | 270 | 180 | 180 | 180 | 90 |
| 16 | - | - | - | 0 | 0 | 180 | 270 | 180 | 90 |
| 17 | 0 | 180 | 270 | - | - | - | - | - | - |
| 18 | 0 | 180 | 0 | - | - | - | - | - | - |
| 19 | 90 | 0 | 90 | - | - | - | - | - | - |
| 20 | 0 | 270 | 0 | - | - | - | - | - | - |
| 21 | 180 | 180 | 180 | - | - | - | 0 | 0 | 270 |
| 22 | 0 | 0 | 0 | - | - | - | 180 | 180 | 90 |
| 23 | 0 | 90 | 90 | - | - | - | 180 | 270 | 180 |
| 24 | 180 | 270 | 270 | - | - | - | 0 | 0 | 0 |

**Table 14 –Phases configurations for the second worst case for all antenna subsets**

| Antenna index | Subset 1 – Base plane Phases [Degrees] | | | Subset 2 –Base plane Phases [Degrees] | | | Subset 3 – Base plane Phases [Degrees] | | |
|---------------|--|--------|--------|---------------------------------------|--------|--------|--|--------|--------|
| | CH1 | CH2 | CH3 | CH1 | CH2 | CH3 | CH1 | CH2 | CH3 |
| | Ph #10 | Ph #11 | Ph #12 | Ph #13 | Ph #14 | Ph #15 | Ph #16 | Ph #17 | Ph #18 |
| 1 | - | - | - | - | - | - | 90 | 180 | 0 |
| 2 | - | - | - | - | - | - | 0 | 0 | 270 |
| 3 | - | - | - | - | - | - | 0 | 0 | 270 |
| 4 | - | - | - | 270 | 0 | 270 | - | - | - |
| 5 | - | - | - | 90 | 180 | 90 | - | - | - |
| 6 | - | - | - | 180 | 0 | 90 | - | - | - |
| 7 | 270 | 0 | 270 | - | - | - | - | - | - |
| 8 | 270 | 0 | 270 | - | - | - | - | - | - |
| 9 | - | - | - | 270 | 90 | 0 | - | - | - |
| 10 | - | - | - | 0 | 90 | 0 | - | - | - |
| 11 | - | - | - | 0 | 90 | 90 | - | - | - |
| 12 | - | - | - | 0 | 180 | 90 | - | - | - |
| 13 | - | - | - | 270 | 0 | 180 | 180 | 180 | 90 |
| 14 | - | - | - | 90 | 180 | 0 | 0 | 0 | 0 |
| 15 | - | - | - | 270 | 0 | 180 | 180 | 180 | 90 |
| 16 | - | - | - | 0 | 0 | 270 | 180 | 270 | 180 |
| 17 | 90 | 0 | 270 | - | - | - | - | - | - |
| 18 | 90 | 90 | 0 | - | - | - | - | - | - |
| 19 | 180 | 180 | 90 | - | - | - | - | - | - |
| 20 | 90 | 90 | 0 | - | - | - | - | - | - |
| 21 | 270 | 180 | 180 | - | - | - | 270 | 0 | 0 |
| 22 | 0 | 0 | 90 | - | - | - | 90 | 180 | 180 |
| 23 | 90 | 90 | 180 | - | - | - | 90 | 270 | 270 |
| 24 | 270 | 180 | 0 | - | - | - | 270 | 90 | 90 |



A.2.3.3 Single-Point power density values in the base evaluation plane

Table 15 presents, for all channels and subsets, the calculated single-point power density values in the base evaluation plane using the first and the second worst-case subset antenna phases presented in Table 13 and Table 14 respectively (18 worst cases).

Table 15 – Maximum single point power density [mW/cm²]

| | First worst case | | | Second worst case | | |
|-----------------|------------------|-----------|-----------|-------------------|-----------|-----------|
| | Channel 1 | Channel 2 | Channel 3 | Channel 1 | Channel 2 | Channel 3 |
| Subset 1 | 1.104 | 0.794 | 0.664 | 1.077 | 0.934 | 0.522 |
| Subset 2 | 0.448 | 0.323 | 0.409 | 0.386 | 0.338 | 0.397 |
| Subset 3 | 2.030 | 2.403 | 1.433 | 2.149 | 1.875 | 1.087 |

A.2.3.4 Spatially averaged power density over 1 cm² values in the base evaluation plane

Table 16 shows, for all channels and subsets, the calculated spatially averaged power density over 1 cm² at 100% duty cycle (eighteen calculated worst cases). These values are calculated in the concerned evaluation plane using the first and the second worst-case subset antenna phases shown in Table 13 and Table 14 respectively.

Table 16 – Maximum spatially averaged power density over 1cm² [mW/cm²]

| | First worst case | | | Second worst case | | |
|-----------------|------------------|-----------|-----------|-------------------|-----------|-----------|
| | Channel 1 | Channel 2 | Channel 3 | Channel 1 | Channel 2 | Channel 3 |
| Subset 1 | 0.263 | 0.211 | 0.109 | 0.221 | 0.157 | 0.108 |
| Subset 2 | 0.072 | 0.069 | 0.068 | 0.066 | 0.067 | 0.066 |
| Subset 3 | 0.395 | 0.336 | 0.168 | 0.382 | 0.271 | 0.137 |

Table 16 shows that the very worst case is found for **subset 3 at channel 1** (marked in orange) with spatially averaged power density of **0.395 mW/cm²** at 100 % duty cycle. The next section presents all power density distributions for this worst cases.

A.2.3.5 Worst case power density distribution

As described in the previous section, the worst case spatially averaged power density over 1 cm² among the eighteen calculated worst-cases is found for subset 3, channel 1. The worst case subset antenna phase's configuration used in this case is for the first worst case (see Table 13, subset 3 / channel 1 configuration).

This section present for this worst case the distribution of the following listed items:

- Upper bound single point power density distribution
- Single-point power density distribution
- One dimensional cut of the single-point power density distribution
- Spatially averaged power density over 1 cm²

Upper-bound power density distribution

Figure 27 presents upper-bound, single-point power density of subset 3, channel 1 which is the worst case among the two simulated worst cases of the three subsets. The evaluation plane of subset 3 is the base plane represented in Figure 17.

The footprint of the platform components in the base evaluation plane for single-point power density representation is shown in Figure 29.

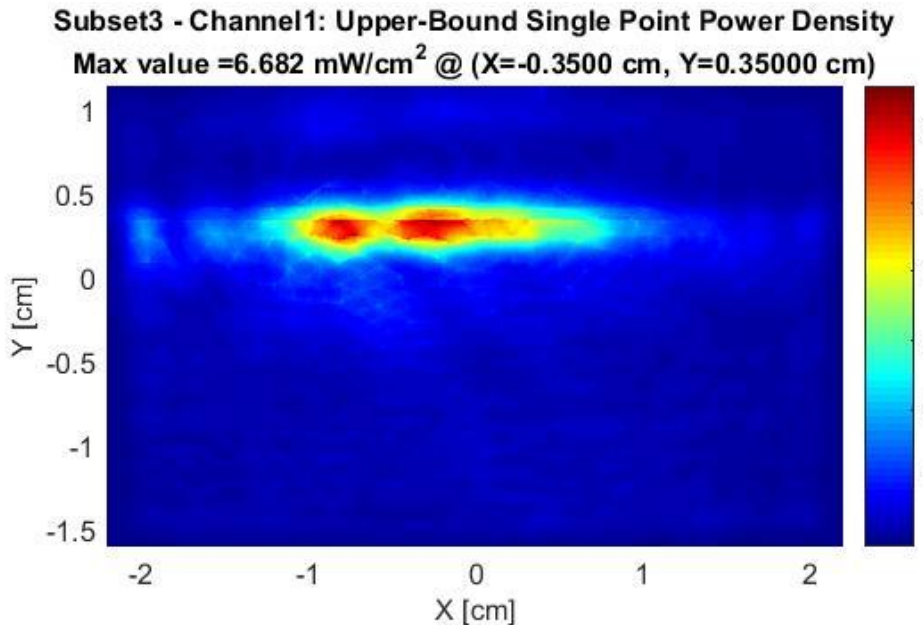


Figure 27 – Channel 3 upper-bound, single-point power density- subset 3

Single point power density distribution

Figure 28 presents the single-point power density distribution of subset 3, channel 1 in the base plane using the worst-case antenna phases (see Table 13, subset 3 / channel 1 configuration)

The footprint of the platform components in the base plane for single-point power density representation is shown in Figure 29.

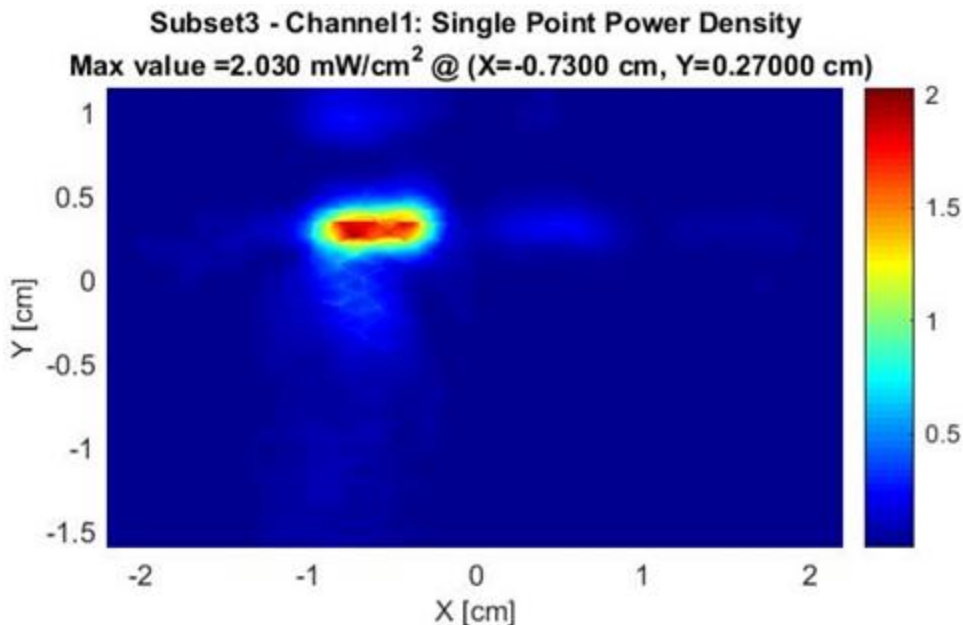


Figure 28 – Channel 3 single-point power density - subset 3

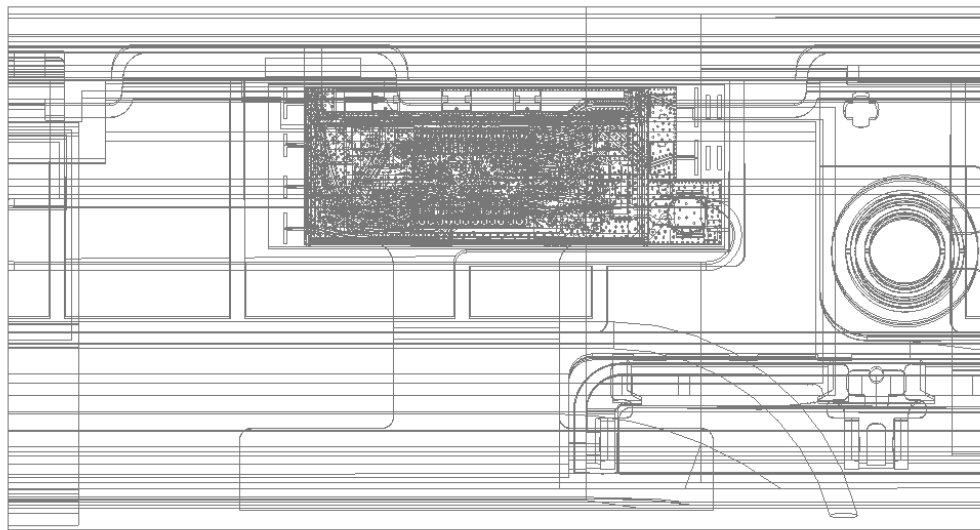


Figure 29 – Footprint of single-point power density plane representation

One dimensional cut of the single-point power density distribution

In Figure 30 and Figure 31, we present the simulation results from the xyz components of single-point power density values with worst-case antenna phases of subset 3, channel 1 which is the worst case among the three subsets. The figures represent a 1-dimensional cut in the x-axis and y-axis that shows the behavior of the near field power density at the evaluation plane.

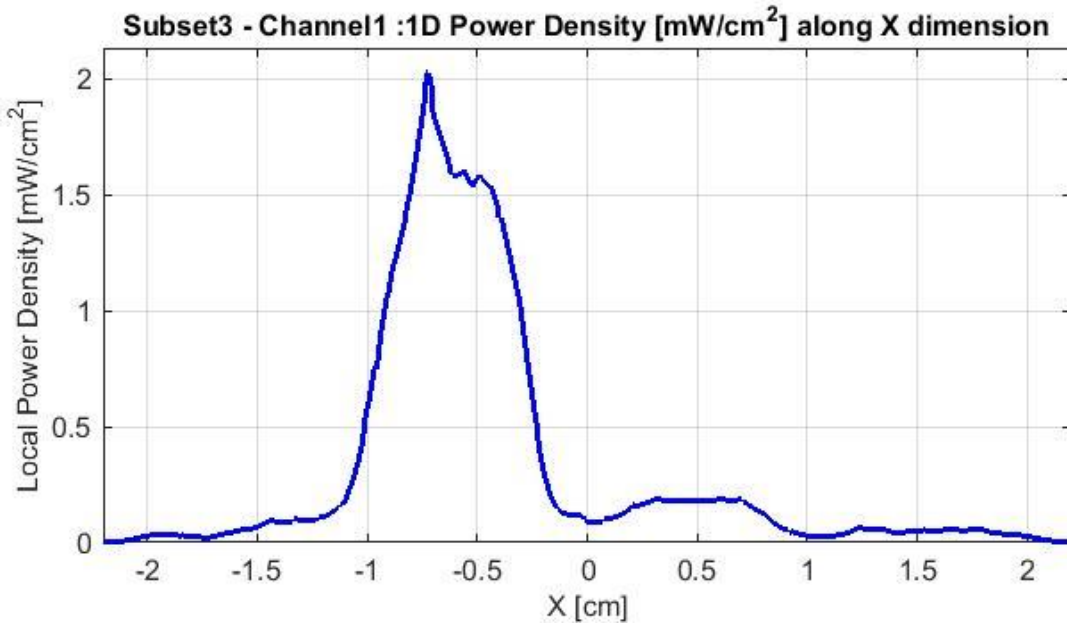


Figure 30 – 1-dimensional plots of the power density along x dimension

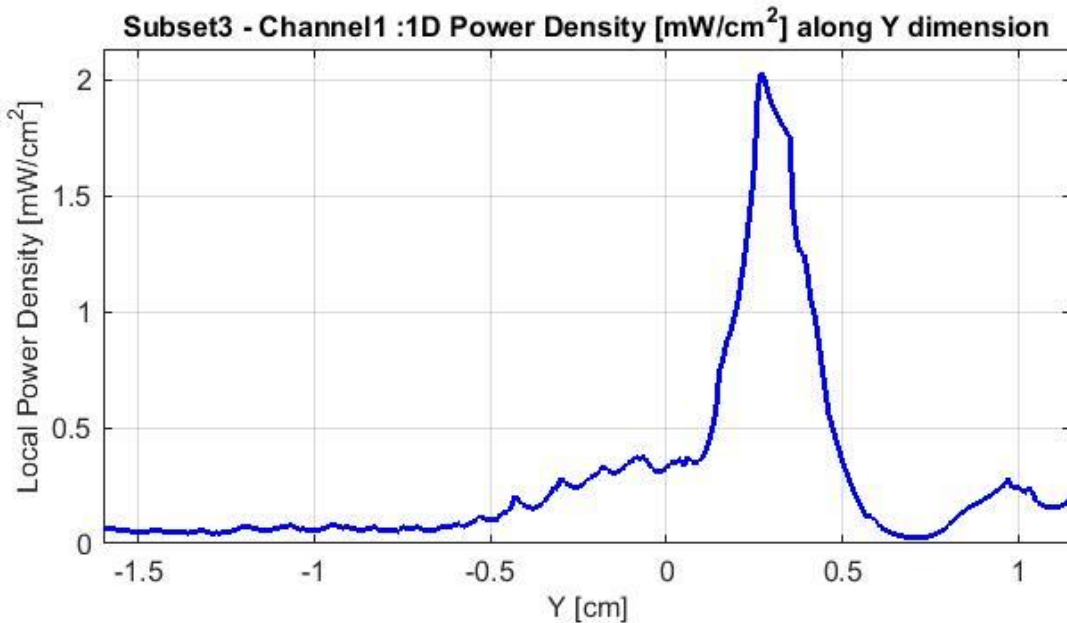


Figure 31 – 1-dimensional plots of the power density along y dimension

Distribution of Spatially averaged power density over 1 cm²

Figure 32 presents the spatially averaged power over 1cm² at 100% duty cycle for the worst-case scenario of subset 3, channel 1 as explained in Section A.1.4.3.

The 1cm² square location correspondent to the maximum of spatially averaged power density value is plotted in Figure 32 for the channel 3.

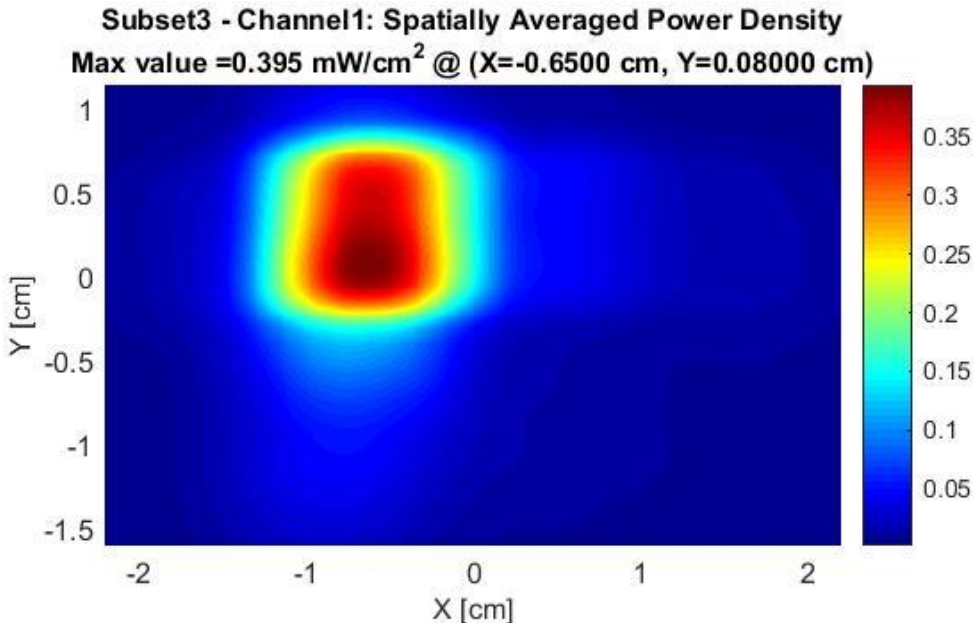


Figure 32 – Channel 1– spatially averaged power density over 1cm2 – subset 3

The Table 17 shows the simulated worst-case power density, for subset 3 – channel 1, in the base evaluation plane.

Table 17 – Worst-case power density – Subset 3

| Highest power density | Subset 3 - Channel 1 |
|------------------------|----------------------|
| 70% duty cycle | 0.276 |
| 100% duty cycle | 0.395 |

Notes for Table 17

4. The worst-case power density is found for channel 1 on subset 3.
5. The Maximum power density (spatially averaged over worst 1cm²) in channel 1 is achieved at 0 mm distance from the platform boundary and equals 0.395 mW/cm² over 100% duty cycle.
6. As explained in Section 2.4, the Intel 18265NGW module is limited to transmit at a duty cycle of 70% over 10 seconds. Therefore the maximum spatially-integrated and time-averaged power density over 1cm² is $0.395 \times 0.7 = 0.276$ mW/cm².



A.2.4 Field and Power Density Distributions for the Six Highest Worst Cases

This section shows the E-field, H-field, local power density and spatially averaged power density distribution at the corresponding evaluation plane of the six highest worst cases spatially averaged power density determined in Section A.2.2.4 and marked in bold in Table 10.

Note: The six highest spatially averaged power density worst case are found in the edge evaluation plane.

The table below list the identified highest six-spatially averaged power density worst cases.

Table 18 – Highest six worst-case spatially averaged power density

| | Evaluation plane | Subset | Channel | Worst-case | Simulated AVG. PD | Phase config. * | Plot |
|---------------|------------------|--------|---------|------------|-------------------|-----------------|---------|
| Worst-Case #1 | Edge | 1 | 1 | 1 | 0.8205 | Ph #1 | Plot #1 |
| Worst-Case #2 | Edge | 1 | 1 | 2 | 0.776 | Ph #10 | Plot #2 |
| Worst-Case #3 | Edge | 1 | 2 | 1 | 0.736 | Ph #2 | Plot #3 |
| Worst-Case #4 | Edge | 2 | 3 | 1 | 0.712 | Ph #6 | Plot #4 |
| Worst-Case #5 | Edge | 2 | 2 | 1 | 0.7 | Ph #5 | Plot #5 |
| Worst-Case #6 | Edge | 1 | 2 | 2 | 0.678 | Ph #14 | Plot #6 |

*See Table 7 and Table 8

Plot # 1: Worst Case 1 - Subset 1 – Channel 1

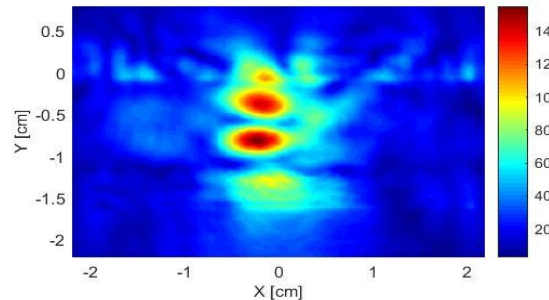
Evaluation Plane: Edge plane

Frequency: 58320 MHz

Distance: 0mm

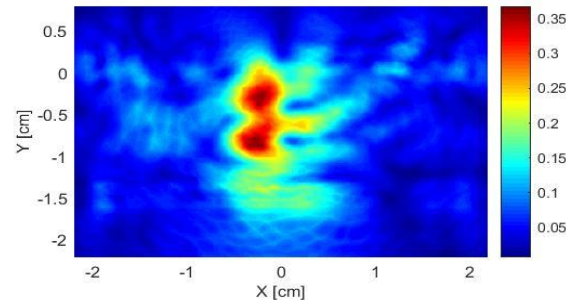
Simulated E-field

Maximum value = 155.349 V/m - Peak



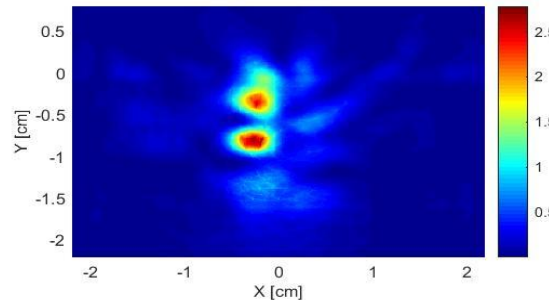
Simulated H-field

Maximum value = 0.368 A/m - Peak



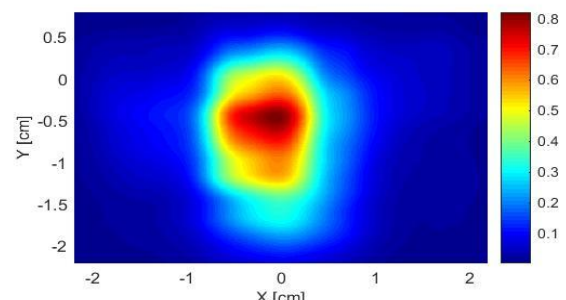
Simulated localized free space power density

Maximum value = 2.783 mW/cm²



Simulated spatially Averaged power density

Maximum value = 0.821 mW/cm²



Plot # 2: Worst Case 2 - Subset 1 – Channel 1

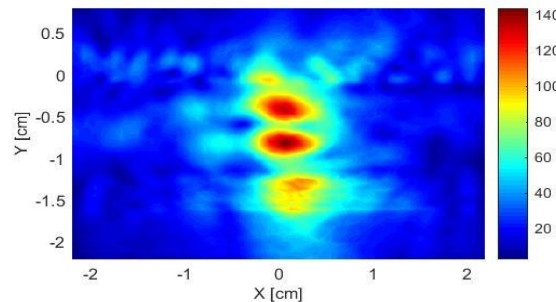
Evaluation Plane: Edge plane

Frequency: 58320 MHz

Distance: 0mm

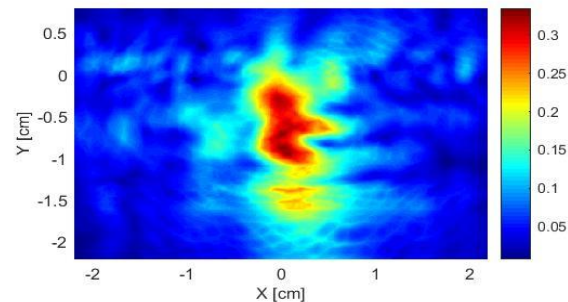
Simulated E-field

Maximum value = 144.051 V/m - Peak



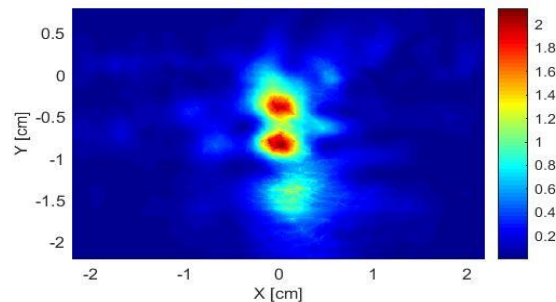
Simulated H-field

Maximum value = 0.335 A/m - Peak



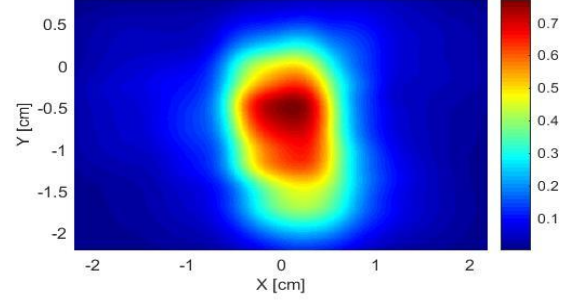
Simulated localized free space power density

Maximum value = 2.139 mW/cm²



Simulated spatially Averaged power density

Maximum value = 0.772 mW/cm²

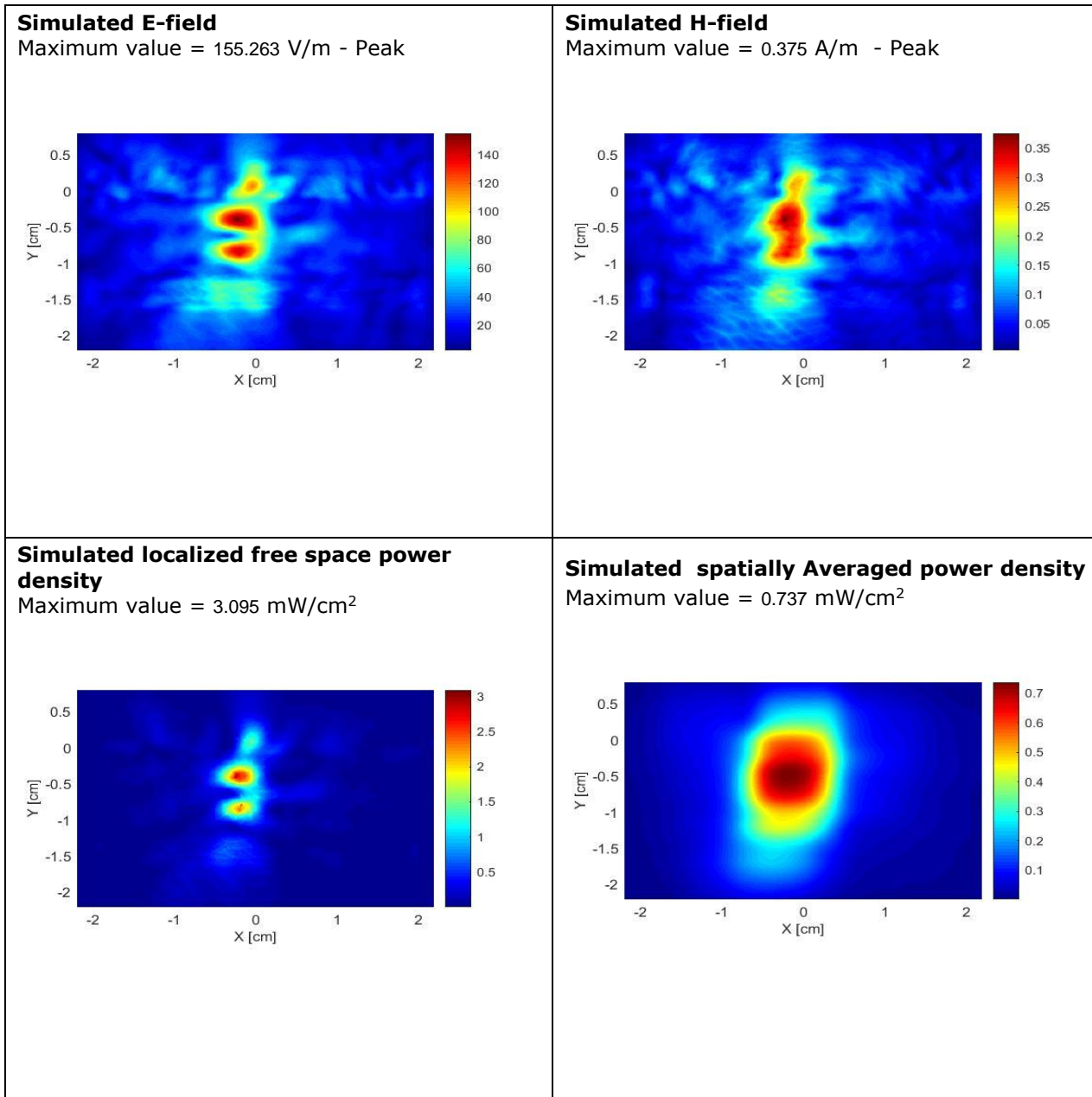


Plot # 3: Worst Case 1 - Subset 1 – Channel 2

Evaluation Plan: Edge plane

Frequency: 60480 MHz

Distance: 0mm

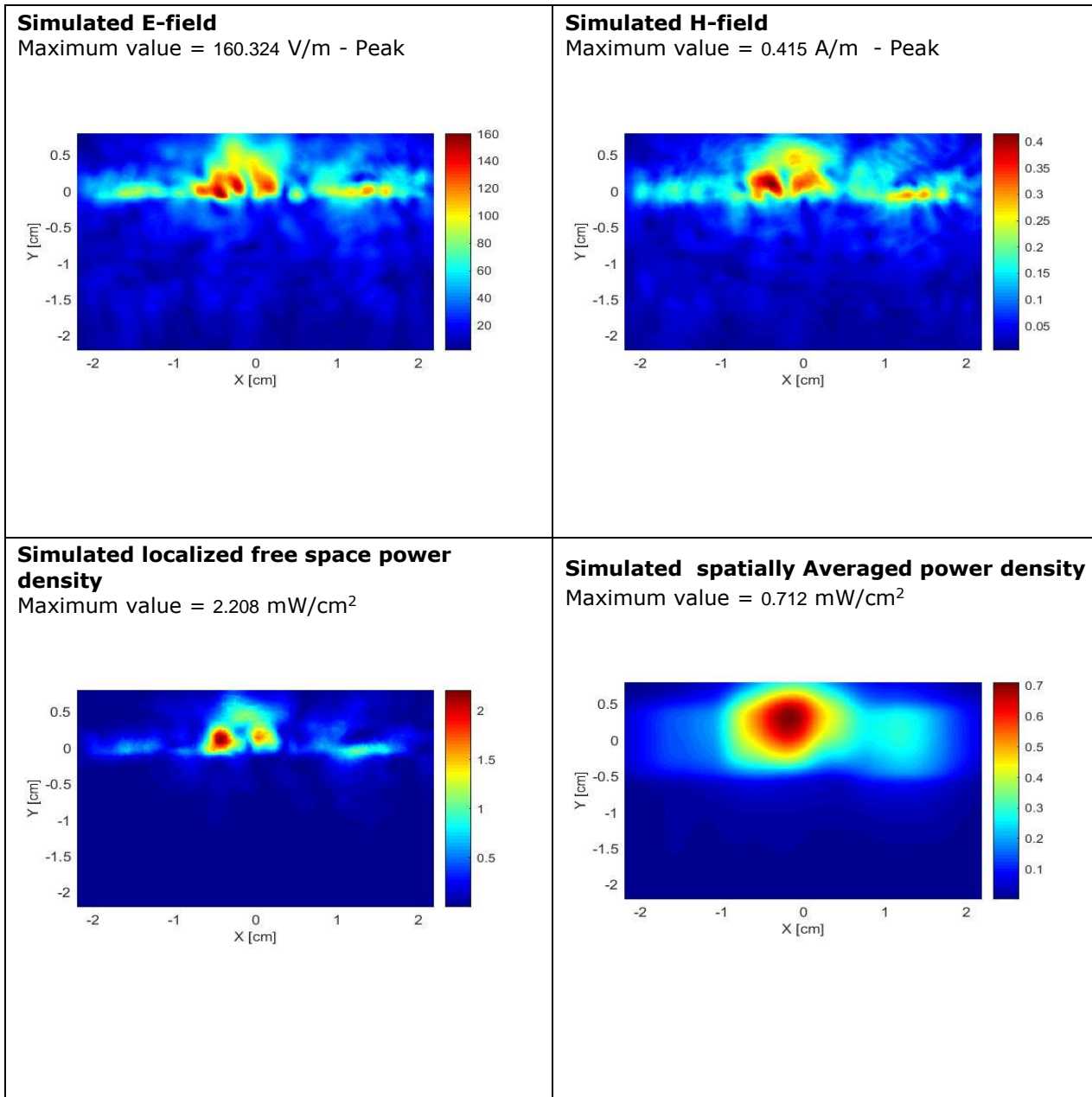


Plot # 4: Worst Case 1 - Subset 2– Channel 3

Evaluation Plan: Edge plane

Frequency: 62640 MHz

Distance: 0mm

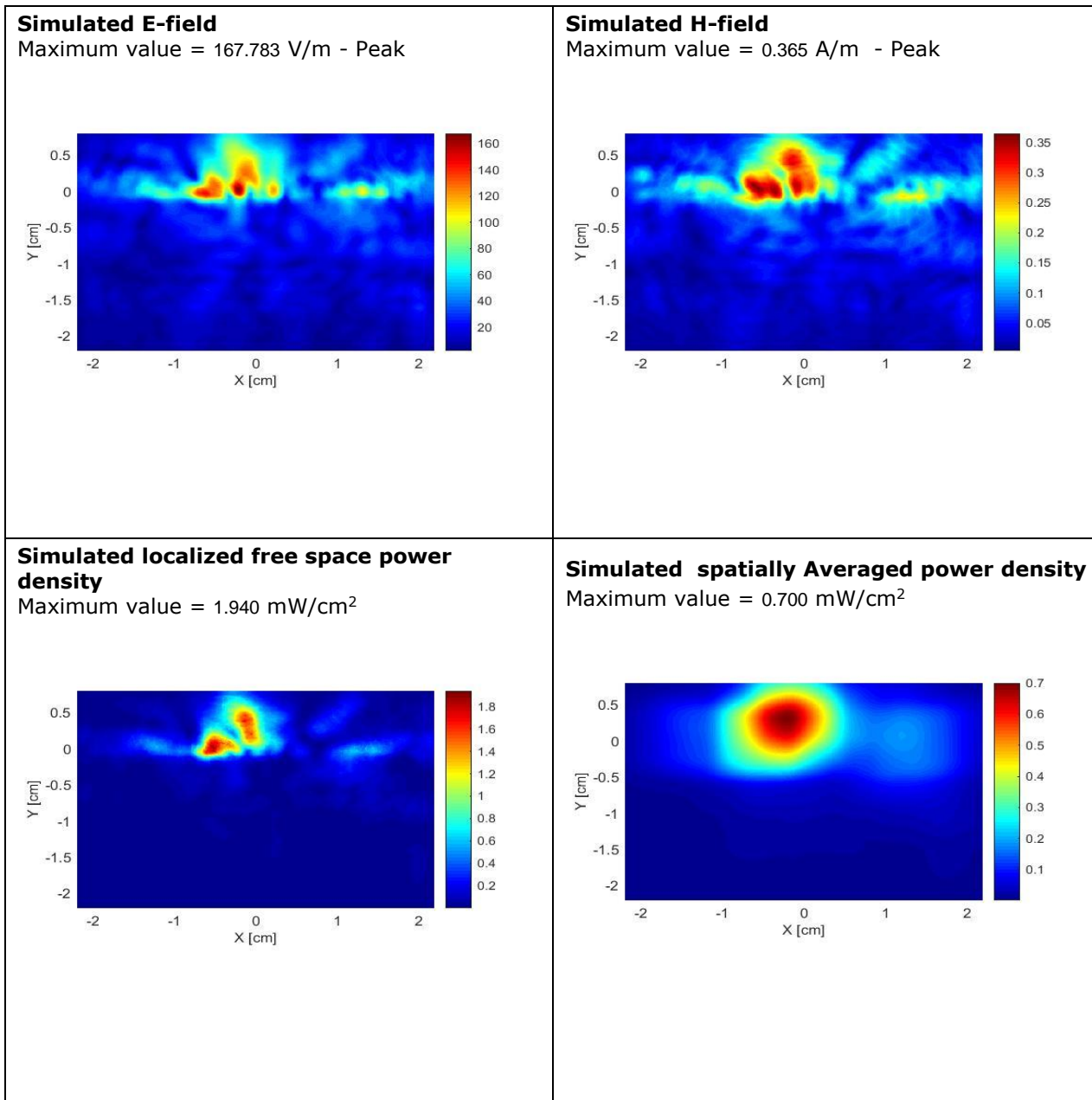


Plot # 5: Worst Case 1 - Subset 2 – Channel 2

Evaluation Plan: Edge Plane

Frequency: 60480 MHz

Distance: 0mm

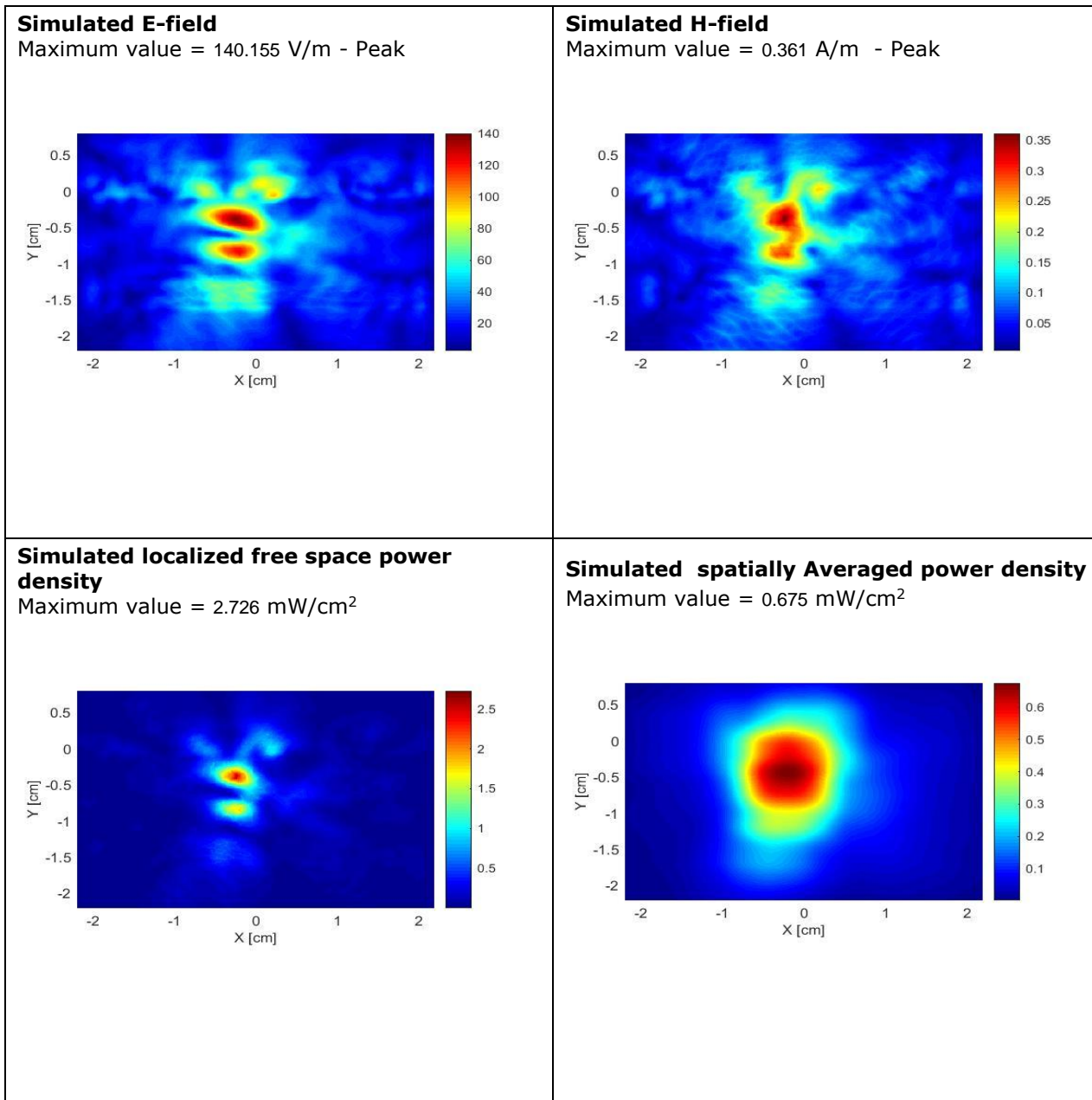


Plot # 6: Worst Case 2 - Subset 1 – Channel 2

Evaluation Plan: Edge Plane

Frequency: 60480 MHz

Distance: 0mm





A.2.5 Conclusion

The simulation results for the three subsets in the edge and the base evaluation planes for three channels were presented in this report. The worst case is observed on the edge plane for channel 3, subset 1, with the maximum total spatially averaged power density of 0.575 mW/cm². Note that the applicable FCC limit is 1 mW/cm².